Molecular Phylogenetics and Evolution 161 (2021) 107181

Contents lists available at ScienceDirect

Molecular Phylogenetics and Evolution

journal homepage: www.elsevier.com/locate/ympev

Phylogeography, historical demography and systematics of the world's smallest pythons (Pythonidae, *Antaresia*)

Damien Esquerré [a,*], Stephen C. Donnellan [b], Carlos J. Pavón-Vázquez [a], Jéssica Fenker [a], J. Scott Keogh [a]

[a] Division of Ecology and Evolution, Research School of Biology, The Australian National University, Canberra, ACT 0200, Australia
[b] South Australian Museum, North Terrace, Adelaide, SA 5000, Australia

ARTICLE INFO

Keywords:
Pythons
Species delimitation
Range expansion
Australia
Morphometrics

ABSTRACT

Advances from empirical studies in phylogeography, systematics and species delimitation highlight the importance of integrative approaches for quantifying taxonomic diversity. Genomic data have greatly improved our ability to discern both systematic diversity and evolutionary history. Here we combine analyses of mitochondrial DNA sequences, thousands of genome-wide SNPs and linear and geometric morphometrics on *Antaresia,* a clade of four currently recognised dwarf pythons from Australia and New Guinea (*Antaresia childreni, A. stimsoni, A. maculosa* and *A. perthensis*). Our integrative analyses of phylogenetics, population structure, species delimitation, historical demography and morphometrics revealed that the true evolutionary diversity is not well reflected in the current appraisal of the diversity of the group. We find that *Antaresia childreni* and *A. stimsoni* comprise a widespread network of populations connected by gene flow and without evidence of species-level divergence among them. However, *A. maculosa* shows considerable genetic structuring which leads us to recognise two subspecies in northeastern Australia and a new species in Torres Strait and New Guinea. These two contrasting cases of over and under estimation of diversity, respectively, illustrate the power of thorough integrative approaches into understanding evolution of biodiversity. Furthermore, our analyses of historical demographic patterns highlight the importance of the Kimberley, Pilbara and Cape York as origins of biodiversity in Australia.

1. Introduction

Until fairly recently, the range of analytical tools available to discover and establish the diversity of species and their evolutionary relationships was focused largely on the visible phenotype of organisms. As a result, many groups are still classified based on their morphological similarity. Often this is has produced an arrangement that is robust in the face of additional evidence, but many evolutionary processes such as stasis and convergence can mislead evolutionary inference and estimates of species diversity. In such cases the real evolutionary history is not apparent from the phenotype and modern genetic tools are needed to uncover it (Fišer et al., 2018; Singhal et al., 2018). The rapid rise and increased accessibility of next generation sequencing allowing us to obtain orders of magnitude more data from genomes, coupled with the development of sophisticated methods to build phylogenetic trees, estimate gene flow, and delineate species, has led to a revolution in the classification of living organisms.

Different lines of evidence, such as those based on phylogenetic relationships, genetic admixture, species delimitation and morphological differentiation point out different patterns and processes that arise at different stages of speciation (De Queiroz, 2007; Mallet, 2008; Sites and Marshall, 2004), which has led to the implementation of more integrative approaches to resolve systematic challenges, known as integrative taxonomy (e.g. Chaplin et al., 2019; Dayrat, 2005; Esquerré et al., 2019; McKay et al., 2014; Padial et al., 2010). For example, relying exclusively on the degree of genetic structuring within a lineage can lead to taxonomic over-splitting (Coates et al., 2018; Sukumaran and Knowles, 2017), which can be a problem for conservation management and macro-evolutionary studies (Coates et al., 2018). The power of large amounts of genomic data translates into the ability to detect very fine patterns of divergence, which need to be interpreted in the appropriate context (Leaché et al., 2018; Pyron et al., 2016). Integrating other sources of evidence into genomic-based approaches often leads to more conservative and realistic interpretations (Esquerré et al., 2019; Pyron

* Corresponding author.
E-mail address: damien.esquerre@anu.edu.au (D. Esquerré).

https://doi.org/10.1016/j.ympev.2021.107181
Received 2 December 2020; Received in revised form 6 April 2021; Accepted 15 April 2021
Available online 21 April 2021

et al., 2016; Solís-Lemus et al., 2015). On the other hand, divergence and speciation are not always coupled with discernible morphological differentiation, and the existence of so called 'cryptic species' is now understood to be common (Fišer et al., 2018; Papakostas et al., 2016; Singhal et al., 2018). Accurate species delimitation is not only important for our understanding of phylogeographic and other evolutionary processes, it is also crucial for conservation and biodiversity assessment (e.g., Devitt et al., 2019; Natusch et al., 2020; Shirley et al., 2014). Finally, advances in the interpretation of population genetic patterns in a geographic context allows us to infer the historical demography of populations, which when interpreted in the context of past climatic and geological events help us understand the processes that have given rise to diversity and its distribution (Bradburd et al., 2018; Peter and Slatkin, 2015; 2013).

Our study is focussed on a genus within the charismatic pythons comprising the snake family Pythonidae (Esquerré et al., 2020). These prey-constricting reptiles include the longest living snakes, with several species growing well over 5 m, and up to 10 m (Murphy and Henderson, 1997). However, within this family of giant snakes, the Australopapuan *Antaresia* represents an intriguing case of dwarfism (Esquerré et al., 2017), where species rarely exceed 140 cm in total length and, in particular, *A. perthensis* very rarely surpasses 70 cm. *Antaresia* comprise a wide-spread, generally abundant, and emblematic group of Australopapuan snakes but our understanding of their evolutionary history is poor. Current taxonomy recognises four species: *A. maculosa* in Queensland and southern New Guinea, the pygmy *A. perthensis* in the Pilbara region of Western Australia and surroundings, and the closely related and morphologically variable *A. childreni* and *A. stimsoni*, widespread through Australia's tropics and subtropics (Esquerré et al., 2020, 2017; Pyron et al., 2013; Rawlings et al., 2008; Reynolds et al., 2014). The morphological diagnosis of these two latter species is based largely on coloration pattern, and, as their pattern is highly variable, researchers often rely on their distributions to identify them, with *A. childreni* found across the Top End in northern Australia and *A. stimsoni* across the more arid regions to the south (Smith, 1985). Additionally, Smith recognised two subspecies of *A. stimsoni*, with *A. stimsoni stimsoni* restricted to the western portion of Western Australia and *A. s. orientalis* across the rest of the species distribution. A more detailed taxonomic history is found in Appendix I.

Despite the utility of morphological characters and single loci in diagnosing the boundaries and relationships between species, integrative frameworks combining numerous lines of evidence are the most valuable tool to increase the accuracy of our understanding of taxonomic richness (Dayrat, 2005; Padial et al., 2010; Papakostas et al., 2016). Here, we analyse mitochondrial (mtDNA) sequences, thousands of short sequences containing single nucleotide polymorphisms (SNPs) coming from the nuclear genome, and geometric and linear morphometrics using a suite of recently developed phylogenetic, population genetic and species delimitation methods to re-assess the systematics of *Antaresia* and understand the evolutionary processes that have led to the group's diversity, biogeographic origins and demographic history.

2. Materials and methods

2.1. Molecular sampling

We gathered 226 tissue samples from the four species of *Antaresia*: *childreni* (n = 91), *maculosa* (n = 37), *perthensis* (n = 15) and *stimsoni* (n = 83), trying to cover as much of the range of each species as possible (see Supplementary Material). We used *Morelia bredli* as an outgroup in phylogenetic analyses (Esquerré et al., 2020). Tissues came from the Australian Biological Tissue Collection (ABTC), the Australian Museum (AMS), the Queensland Museum (QM), the Western Australia Museum (WAM) and a few from private collections. We extracted DNA using either a Qiagen DNeasy Blood & Tissue kit or a salt extraction protocol (Miller et al., 1988).

We obtained mtDNA sequences of the *cytochrome b* (*cyt-b*) gene for 117 individuals following the protocol in Natusch et al. (2020). We checked and edited sequences using Geneious Prime 2020 (Biomatters, Auckland, New Zealand, 2019) and aligned them using MAFFT v.7.309 (Katoh and Standley, 2013). Mitochondrial sequences are available from GenBank (Accession numbers in supplementary data on *Dryad*). For nuclear DNA (nDNA) genotyping, we sent 187 tissue samples to Diversity Arrays Technology (DArTSeq; Canberra, Australia), who performed a genome complexity reduction technique using specific restriction enzymes (PstI and HpaII) and sequenced the DNA fragments on an Illumina HiSeq2500 sequencer (CA, USA). DArTSeq apply proprietary pipelines to filter polymorphic loci for quality and reproducibility delivering a matrix of single nucleotide polymorphisms (SNPs) and their associated sequence tags (Georges et al., 2018; Kilian et al., 2012), which yielded 65,741 sequences containing 103,508 SNPs. Our nuclear sequence data is available on *Dryad,* raw reads and statistics (i.e., call rate, polymorphic information content, heterozygosity, read depth, and reproducibility for all loci and individuals) are accessible from Diversity Array Technology Pty. Ltd., Canberra, Australia (Report-DAnte18-3811)

Using the R package *dartR* (Gruber et al., 2018), these SNP data were filtered further (in the following order) by call rate (removing loci with more than 10% missing data), minor allele frequencies (removing loci with minor allele frequency lower than 0.005), reproducibility (keeping SNPs present in 100% of replicates), read depth (removing loci with<5x coverage), removing monomorphic loci and keeping only one SNP per locus, resulting in 11,841 SNPs. We used a combination of *dartR* and Geneious Prime for alignment format conversion for downstream analysis. For some downstream analyses where we aimed at maximising the number of loci for *A. childreni / A. stimsoni* or *A. maculosa*, we performed independent SNP data filtering for these taxa alone, which resulted in 12,615 and 5,385 SNPs, respectively.

2.2. Phylogenetic hypotheses

To infer the mtDNA gene tree based on *cyt-b*, we first estimated the optimal codon partitioning scheme and substitution model for each partition using the ModelFinder algorithm implemented in *IQ-Tree* v. 1.7 (Chernomor et al., 2016; Kalyaanamoorthy et al., 2017; Nguyen et al., 2015), which found a different substitution model for each codon position. These were used to infer a maximum likelihood (ML) tree in *IQ-Tree*, summarizing phylogenetic uncertainty with 1,000 ultrafast bootstraps (Hoang et al., 2018), and gene (in this case codon; gCFs) and site (sCFs) concordance factors (Minh et al., 2018).

To infer phylogenetic trees using the nDNA we used two approaches. First, using the concatenated sequence tags (the sequences that contain the SNPs), we used ModelFinder to find the optimal substitution model according to the Bayesian Information Criterion (BIC). This was an HKY model with empirical base frequencies and a FreeRate model (Soubrier et al., 2012) with two categories (HKY + F + R2). We inferred the maximum likelihood tree and 1,000 ultrafast bootstraps using *IQ-Tree*. Second, we used the SNPs to model a lineage tree based on the multispecies coalescent. We used the program *SVDQuartets* (Chifman and Kubatko, 2014), implemented in PAUP v. 4.0 (Swofford, 2003) and we conducted separate analyses for *Antaresia maculosa* and *A. children/stimsoni* to make computational times feasible. The software computes all possible four-taxon quartets, assuming each site is independent, and accounting for incomplete lineage sorting. We assessed branch support with 100 bootstrap replicates.

2.3. Population structure

We performed the following analyses using the nuclear SNPs. First, to visualise genetic clusters and their correspondence to clades found with phylogenetic analyses, we performed principal coordinates analyses (PCoA). Then, to assess population structure and ancestry we used

the likelihood-based program *sNMF* (Frichot et al., 2014). This program provides a fast and efficient algorithm to estimate the optimal number of genetic clusters (K) and the ancestry coefficients of the individuals. We optimised the tolerance and alpha (regularisation) parameters by running *sNMF* on our dataset with K from 1 to 12 and choosing the combination that minimised the cross entropy, which was a tolerance = 0.000001 and alpha = 0. With these parameters we ran *sNMF* 100 times and chose the run and K with the lowest cross entropy, which estimated K = 8. Finally, we repeated the above procedure with the *childreni/stimsoni* and the *maculosa* independent datasets to assess the partitioning of genetic structure at a finer scale. We found the optimal K for these datasets to be six and three, respectively.

The identification of discrete genetic clusters may be confounded by the presence of isolation by distance (IBD), which appears to be a widespread pattern in nature (Bradburd et al., 2018; Sexton et al., 2013). We used two approaches to investigate the presence of IBD as the model of genetic population structure in the *maculosa* and *childreni/stimsoni* clades: a Mantel test between geographic and genetic distances, and *conStruct* (Bradburd et al., 2018), a Bayesian method that incorporates IBD into the estimation of admixture proportions.

Mantel tests of IBD are usually performed on F_{ST} / 1 − F_{ST}, but localities in our dataset are mostly represented by a single individual, rendering F_{ST} inaccurate. Thus, we calculated the $\hat{a}$ statistic (Rousset, 2000) between pairs of individuals in *genepop* v. 1.1.7 (Rousset, 2000) and used it as our measure of genetic distance. Our measure of geographic distance was the log-transformed Euclidean distance between collection locations in the Mercator projection. We performed the Mantel test in *dartR* and assessed significance through 1,000 permutations.

Preliminary *conStruct* runs including all the individuals belonging to each clade mixed poorly. Thus, we collapsed localities that were <100 km away from each other into a single sample and calculated allele frequencies accordingly using custom scripts available at https://github.com/CarlosPavonV/RandomMolR. We calculated pairwise geographic distances as the log-transformed orthodromic distances between collecting localities. We deleted individuals and loci with more than 15% missing data due to the sensitivity of *conStruct* (Barley et al., 2019). For the analysis of the *childreni/stimsoni* and *maculosa* clades we reduced our dataset to 35 and 11 localities, respectively, to decrease computation times. The filtering applied here resulted in 12,593 and 5,183 loci for the *childreni/stimsoni* and *maculosa* clades, respectively. Analyses were performed in *conStruct* v. 1.0.5 (Bradburd et al., 2018). We ran cross-validation analyses with three replicates for each value of *K* between 1 and 5 in *maculosa,* each replicate comprising 100,000 iterations and using 90% of the data in the training stage for both a spatially informed and a non-spatial model.

Preliminary *conStruct* analyses of the *childreni/stimsoni* clade showed that, for values of *K* larger than three, computation times became prohibitive. In addition, preliminary analyses showed that layer contributions for values of *K* above two were minimal, and that 30,000 iterations were enough to reach consistent results across replicates. Thus, the analyses of the *childreni/stimsoni* clade comprised 30,000 iterations for values of *K* between 1 and 3. We chose between the spatial and non-spatial models based on their predictive accuracy (Fig. S6) and estimated layer contributions to select the optimal value of *K* (Fig. S7). For the preferred model and value of *K*, we first verified that the estimated admixture proportions were similar across runs and then calculated the mean admixture proportions for each individual.

2.4. Species delimitation

We used a fixed differences analysis (Georges et al., 2018) to quantify the number of loci showing fixed allele differences (two clades not sharing an allele at a locus) between the identified clades, as this is a simple yet reliable indicator of lack of gene flow, particularly with the large sample sizes we are using (except for *maculosa* c – see Results). We used the *gl.collapse.recursive* function from R package *dartR* which first amalgamates populations or clades with no fixed differences between them into one and then performs pairwise comparisons of fixed differences between groups. It then performs simulations to estimate the expected number of false positives and compares it to the observed count of loci showing fixed differences for each comparison, providing a *P* value for the statistical significance of the observed differences. We performed this for the whole dataset and for the *childreni/stimsoni* and the *maculosa* datasets independently.

Additionally, we inferred the genealogical divergence index (gdi) (Jackson et al., 2017), that estimates the amount of genetic divergence between two taxa, with values ranging from 0 (complete panmixia: strong support for same species) to 1 (complete divergence: strong support for different species). Leaché et al. (2018) proposed the use of the posterior estimates of ancestral population size (θ) and divergence times (τ) from the multi-species coalescent (MSC) program *BPP* to compute the gdi for each pair of sister taxa. We ran *BPP* v 4.2 (Flouri et al., 2018) with a fixed topology and species delimitation on three scenarios based on our phylogenetic hypotheses (see Results), to calculate the gdi between each pair of sister candidate taxa: 1- ((*maculosa* c,(*maculosa* a, *maculosa* b)),(*perthensis*,((clade 1a, clade 1b),(clade 2a, clade 2b)))); 2 - (*maculosa* c, *maculosa* a + b), (*perthensis*, (clade 1, clade 2)); and 3 - *maculosa*, (*perthensis*, *stimsoni/childreni*). Because of the large dataset and the computational demands of an MSC-based and Bayesian program like BPP we subsampled 600 random loci. We defined priors for the ancestral population size (θ_0) and root age (τ_0) with *inverse gamma* (3, 0.002) and *inverse gamma* (3, 0.005), based on the observed sequence divergence within and between populations, respectively. We ran the reversible jump (rj) MCMC for 500,000 generations, with a burnin of 32,000 and a sampling frequency of five. We performed each analysis twice to confirm convergence between the runs. We then computed the gdi for each taxon with the formula $1 - e^{-2\tau AB/\theta A}$, where τAB corresponds to the divergence time between the that taxon and its sister taxon, and θA to the ancenstral population size of the target taxon. Values below 0.2 are considered strong support for a single species, and above 0.7 strong support for distinct species, whereas values between these two indicate uncertain or ambiguous delimitation (Jackson et al., 2017; Leaché et al., 2018).

2.5. Divergence times

To estimate divergence times between clades, we used *bbpr* v.0.6, an R package that can convert relative divergence times (τ) estimated by *BPP* to geological timescale, by sampling from a node prior (Angelis and Reis, 2015; Yoder et al., 2016). We used the posterior estimates from the full BPP analysis described above and a secondary calibration for the crown age of *Antaresia*, specifying a uniform prior between 11.2 and 14.5 Mya (Esquerré et al., 2020).

2.6. Historical demography

We calculated the genetic diversity indices of observed heterozygosity (Ho) and Tajima's D (Tajima, 1989) for the clades identified in the analyses described above. Elevated Ho values are indicative of admixture and/or large effective population size. Ho was calculated using the R package *dartR* (Gruber et al., 2018), including a estimation of invariant loci to allow comparability across species. Tajima's D is used to estimate departures from neutral mutation-drift equilibrium, with negative values indicating an excess of rare alleles (expected from population expansion) and positive values a loss of rare alleles (expected from population bottlenecks), compared to a neutral model (Tajima, 1989).

We tested for range expansion following the approach described by Peter and Slatkin (Peter and Slatkin, 2015, 2013), using the R package *rangeexpansion* (Peter, 2017). This approach uses a stepping stone model of population expansion from a single population and compares it with

an equilibrium expected by an isolation-by-distance model. If a sign of population expansion is detected, it will calculate the strength of the founder effect during expansion, as well as the likely origin of expansion. We used the sister taxa of each species as an outgroup to calculate the derived state of the SNPs for each species and clades (Potter et al., 2016), needed to run the analyses. We excluded *maculosa* c from these demographic analyses since it only includes two samples.

2.7. Morphometric sampling

To quantify and analyse phenotypic variation amongst the apparently isolated clades that we identified with the molecular data, we used three approaches. To quantify dorsal head shape, we used two-dimensional geometric morphometrics, using 205 specimens from all *Antaresia* clades with sample sizes of: *perthensis* (n = 39), *childreni/stimsoni* clade 1 (n = 14), *childreni/stimsoni* clade 2 (n = 113), *maculosa* a (n = 8), *maculosa* b (n = 27) and *maculosa* c (n = 4). Landmark digitising and Procrustes analyses followed Esquerré and Keogh (2016) and Esquerré et al. (2017).

To quantify body shape, we improved geographic sampling by including the measurement data from Smith (1985), after confirming that the measurements were consistent for specimens that we also measured. We also added data for a specimen from Weam, Papua New Guinea, described by O'Shea et al. (2004). This increased our sampling to 631 specimens comprising *perthensis* (n = 79), *childreni/stimsoni* clade 1 (n = 122), *childreni/stimsoni* clade 2 (n = 329), *maculosa* a (n = 23), *maculosa* b (n = 73), and *maculosa* c (n = 5). For all analyses except for scale counts, we removed juveniles as per Esquerré et al. (2017), reducing the sampling to 485 specimens: *perthensis* (n = 56), *childreni/stimsoni* clade 1 (n = 99), *childreni/stimsoni* clade 2 (n = 255), *maculosa* a (n = 16), *maculosa* b (n = 56), and *maculosa* c (n = 3). We took the following six morphometric measurements for the specimens listed above: snout-vent length (SVL), tail length (TL), mid-body girth, neck girth, head width and head length, as described in Esquerré et al. (2017). Finally, to estimate variation in lepidosis (scalation) we recorded the following scale counts: ventrals, subcaudals, post-oculars, loreals, supralabials and infralabials. We also counted the infralabial heat pits. Some characters could not be measured for all specimens (e.g. incomplete tails, damaged scales), and thus to allow the implementation of the analyses described below, we imputed these missing data using a random forest machine learning algorithm using clade and the morphometric measurements as predictors, implemented in the R package *missForest* (Stekhoven and Bühlmann, 2012).

2.8. Morphometric analyses

To remove the effect of scale on the data, we computed the log-shape ratio of each linear measurement (Claude, 2013), which simply controls for the effect of scale, rather than allometry, unlike using the residuals of a regression on size that assumes equal linear relationships of all measurements with size between species (Esquerré et al., 2017; Klingenberg, 2016). We tested for the effect of sex and clade using a multivariate linear model, then performed pairwise comparisons between the clades, and assessed the statistical significance with a residual randomisation of 10,000 iterations. This was performed using the R package *RRPP* (Collyer and Adams, 2018). To visualize the phenotypic variation between clades and the main characters that explain this variation, we performed principal components analyses (PCA), using the R packages *FactoMineR* (Lê et al., 2008) for the linear morphometrics and *geomorph* (Adams et al., 2016) for the geometric morphometrics. Finally, we plotted kernel density plots to visualise variation in lepidosis per clade.

To assess the coloration and pattern variation according to the established genetic lineages for identification purposes, we gathered photographs of live specimens across their range and qualitatively described the variation.

3. Results

3.1. Phylogenetic hypotheses

All analyses recover *Antaresia maculosa* as the sister lineage to the other species and *A. perthensis* as the sister species to *A. children* and *A. stimsoni* (Fig. 1 and see Figs. S1-4). We found three well-supported clades of *A. maculosa* geographically distributed from north to south. First, the northernmost clade (which we call *maculosa* c) is the sister to the two remaining clades and is formed by the samples from Sota, New Guinea and Moa Island in the Torres Strait (we did not have mtDNA data for these samples). Second, we infer a Cape York clade conformed by populations from the northern portion of Cape York to around Cairns (*maculosa* a). Finally, the third and southernmost clade comprises central and southern Queensland populations ranging from the Paluma Ranges south of Cape York to around Roma in southern Queensland (*maculosa* b).

The phylogeographic structure of *Antaresia childreni* and *A. stimsoni* is not congruent with current taxonomy. Current taxonomy places *A. childreni* in the Top End, Kimberley and the western part of the Gulf of Carpentaria and *A. stimsoni* with a wide distribution in arid and semi-arid Australia excluding the extreme north and south, marginally overlapping with each other (Fig. 1). Both our mtDNA and nDNA data support two main clades of *A. childreni / stimsoni* but with very different distributions compared with prior notions based on the current taxonomy.

Clade 1 is distributed widely across Western Australia and contains two main subclades: clade 1a occurs from around Broome in the southern Kimberley down across much of Western Australia and clade 1b is distributed across the northern part of the Kimberley. The sample from Irvine Island off the Kimberley coast is inferred as sister to clades 1a and 1b by the species tree, as part of clade 1a by the mtDNA and as part of clade 1b by the nDNA gene tree. The most notable discordance between mtDNA and nDNA is the placement of a sample from the King Edward River in the northern Kimberley and a few samples from the Kimberley islands, which are inferred as part of clade 2a by mtDNA and 1b by nDNA.

Clade 2 occurs mostly in the eastern side of the range of *Antaresia childreni / stimsoni*, starting around the eastern end of the Kimberley, across Northern Territory's Top End, the Gulf of Carpentaria into Cape York at its north-eastern margin, encompassing all the populations in Queensland, New South Wales and South Australia in the south. Interestingly, on the southwestern margin of the distribution of clade 2, populations go further west than the eastern limits of clade 1, as far as the Gibson Desert, suggesting possible overlap between both lineages. The subclade structure of clade 2 is much less resolved and more discordant between analyses than in clade 1.

3.2. Population structure

Since the results from analyses of the whole dataset, and also those for separate lineages, are highly concordant, we discuss the results based on the whole dataset here and point out discrepancies with the other analyses when needed. Population genetic structure is highly concordant with our phylogenetic results (Figs. 1 and 2). The PCoA of all of our samples reveals that the first axis (explaining 69% of the variation) separates the samples into two broad groups: *Antaresia childreni / stimsoni* and *A. perthensis* in one and *A. maculosa* in the other, while the second axis (6% of variation) separates *A. perthensis* from the rest (Fig. 2A). On the third axis (3.2% of variation) we see a separation of the three *A. maculosa* clades, with *maculosa* b being the most divergent. When analysing only *A. childreni / stimsoni* samples we see that genetic variation is more spread across axes. The first axis (15.6% of variation) separates clades 1 and 2, but the individuals are not tightly clustered suggesting little genetic isolation (Fig. 2B). The second axis (8.9% of variation) separates clades 1a and 1b, while the remaining axes do not

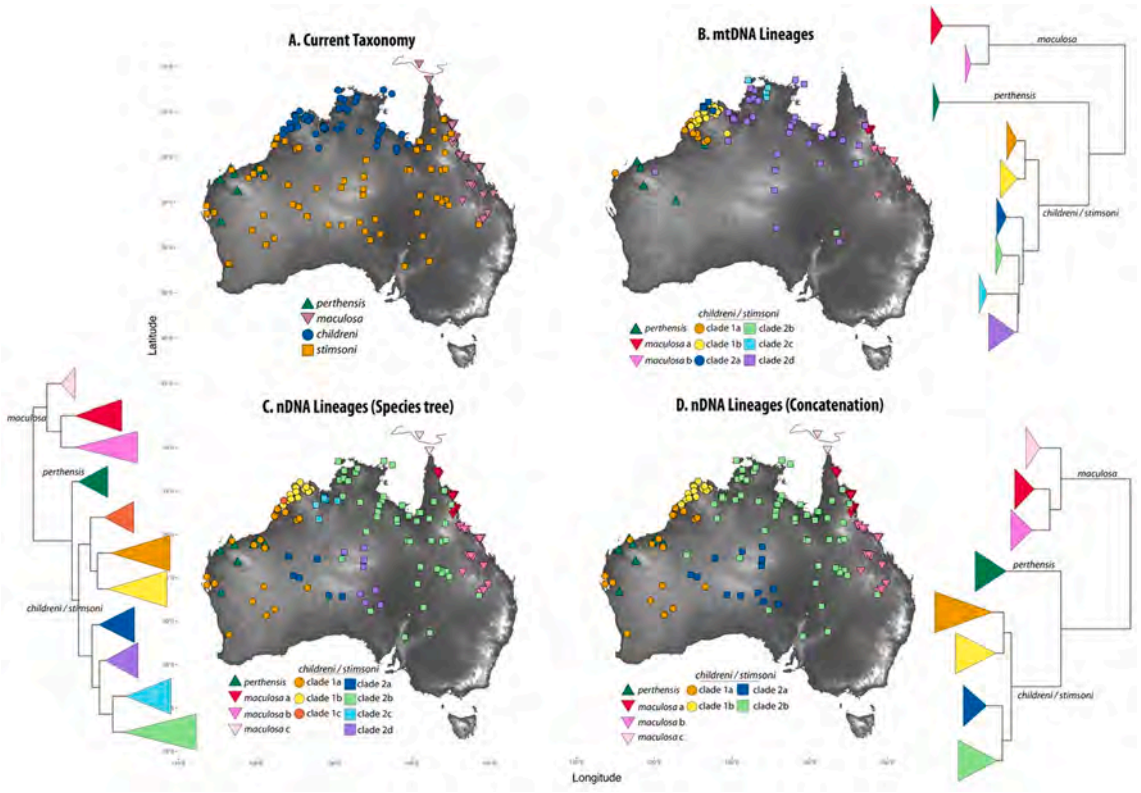

Fig. 1. Distribution maps of samples, colored by **A**: current taxonomy. **B**: mithocondrial DNA (mtDNA) lineages. **C**: nuclear DNA (nDNA) lineages based on a species tree (inferred with SVDQuartets). **D**: nDNA lineages based on maximum likelihood gene tree inference (with IQ-Tree). Trees next to the maps illustrate the relationships between the clades.

clearly separate clades, indicating high intra-clade genetic variation in relation to inter-clade variation. When analysing only *A. maculosa* we see that the first PCoA axis (40.1% of variation) mostly separates the samples into *maculosa* a + *maculosa* c and *maculosa* b, while the second axis (16.7% of variation) separates *maculosa* c from the rest (Fig. 2C).

In the ancestral coefficient analysis (with *sNMF*) of all the samples, the optimal number of populations (K) was eight (Fig. S5). We observe very little admixture between *A. childreni / stimsoni*, *A. maculosa* and *A. perthensis*. Within *A. maculosa,* clades *maculosa* a (Cape York) and *maculosa* b (central/southern Queensland) display strong genetic structure, while *maculosa* c (Torres Straight and New Guinea) shows admixture from both previous clades. However, when *A. maculosa* is analysed separately, we do find three genetic clusters, each representing one of the clades, with a little admixture observed at samples geographically adjacent to the edges of the clade geographic boundaries (Fig. 3).

The structure of *A. childreni / stimsoni* is more complex, with patterns of admixture that suggest gene flow between clades. Clades 1a (central and southern Western Australia) and 1b (Kimberley) display strong genetic structure, but some admixture occurs in some of the Kimberley islands, such as Irvine, Kingfisher and Lachlan Islands (Figs 3 and S5). Clade 1a also shows considerable admixture with clade 2a, particularly between populations in the Pilbara and central Western Australia. Clades 2a and 2b show little genetic structure, suggesting considerable gene flow between lineages, particularly where they are in close proximity in central Australia, the Gulf of Carpentaria and central-western Queensland.

The Mantel test between geographic and genetic distances was significant for both lineages (*A. maculosa*, $r = 0.64$, $P = 0.001$; *childreni / stimsoni*, $r = 0.4$, $P = 0.001$; see Table S1 for test results for individual subclades). However, Mantel tests are prone to type I error (Diniz-Filho et al., 2013) and visual exploration of the data is usually fruitful. In *A. maculosa* geographic structure is apparent: genetic distance relative to geographic distance is larger between *maculosa* a and *maculosa* b than within clades, and even larger when comparing *maculosa* c with *maculosa* a and *maculosa* b (Fig. 4). However, geographic and genetic distances appear to be correlated in between-clade comparisons, suggesting recent divergence and/or admixture near contact zones. In the *childreni / stimsoni* clade discrete structure is less evident and geographic and genetic differences do not appear to be linearly correlated. Mantel tests within each subclade of *A. maculosa* and *childreni / stimsoni* were significant, with IBD being more evident within clades *maculosa* a, *maculosa* b, and *childreni / stimsoni* 2a (Fig. 4 and Table S1).

The *conStruct* analyses generally estimated higher levels of admixture than *sNMF* (Fig. 5). The spatially-informed model generally performed better than the non-spatial model in all the analyses (Fig. S6). In the case of *A. maculosa*, the predictive accuracy plateaued at $K = 3$ (Fig. S6) and, in two of the runs for values of K above three, new layer contributions where minimal (Fig. S7). In contrast with the *sNMF* results, members of *maculosa* a show high levels of admixture with *maculosa b*. Levels of admixture between *maculosa* c and the other clades remained low. In the case of the *childreni / stimsoni* clade, the predictive accuracy increased little for values of K above two, and in all runs where $K = 3$, new layer contributions were minimal. The populations recovered by *conStruct* when $K = 2$ are equivalent to clades 1 and 2, and show high levels of admixture where they come into contact in eastern Western Australia and western Northern Territory (Fig. 5).

3.3. Species delimitation

The fixed differences analysis found no loci showing fixed allelic differences between any of the *Antaresia childreni/stimsoni* clades (even when analysed independently from *A. maculosa* and *A. perthensis*), but hundreds between this clade and *A. perthensis* and all three *A. maculosa*

Fig. 2. Principal Coordinates Analyses of the SNPs called for **A**: the whole dataset, **B**: the *childreni / stimsoni* dataset, and **C**: for the *maculosa* dataset. Individuals are coloured according to their nDNA clades. Each axis has the percentage of variance it explains.

clades (Table 1). Moreover, the three *maculosa* clades also had a high number of loci showing fixed differences between them. All of these comparisons were highly significant ($P < 0.0001$).

The gdi indicate strong support for genetic divergence in *Antaresia perthensis, A. maculosa* and *maculosa* c, with posterior estimates consistently over 0.7 (Fig. 6). Values for *childreni/stimsoni*, *maculosa* a and *maculosa* b are moderate, with values between 0.4 and 0.7, and values for all *childreni/stimsoni* subclades as well as the clade formed by *maculosa* a + b are low (generally below 0.2), indicating low genetic divergence (Fig. 6).

3.4. Divergence times

We estimate an initial divergence of *Antaresia* between *maculosa* and the rest in the mid-Miocene (12.85 Mya; 95% HPD (high posterior density) 14.49–11.36 Mya) (Fig. 7). The divergence between *maculosa* c and *maculosa* a + b (3.08 Mya; 95% HPD 4.26–1.99 Mya) and the divergence between *maculosa* a and b (2.24 Mya; 95% HPD 3.15–1.47 Mya) are inferred in the Pliocene. The divergence between *perthensis* and *childreni/stimsoni* is inferred in the late Miocene (7.32 Mya; 95% HPD 9.54–5.29 Mya) and the divergence between *childreni/stimsoni* clades 1 and 2 in inferred in the Pleistocene (1.3 Mya; 95% HPD 1.54–1.06 Mya) (Fig. 7).

3.5. Historical demography

Mean Ho values varied between 0.005 and 0.014 (Table 2). All species presented negative Tajima's D values (-0.204 to −1.093; Table 2), indicating recent population expansion, with *Antaresia childreni/stimsoni* as a whole and clade 2 showing the most negative values. The range expansion model using the Peter and Slatkin (2013) approach was supported for *A. childreni/stimsoni* and *A. perthensis* (Table 2). When the analyses were performed at the clade level, we observed signs of expansion for *childreni/stimsoni* clade 2 and the combined clade of

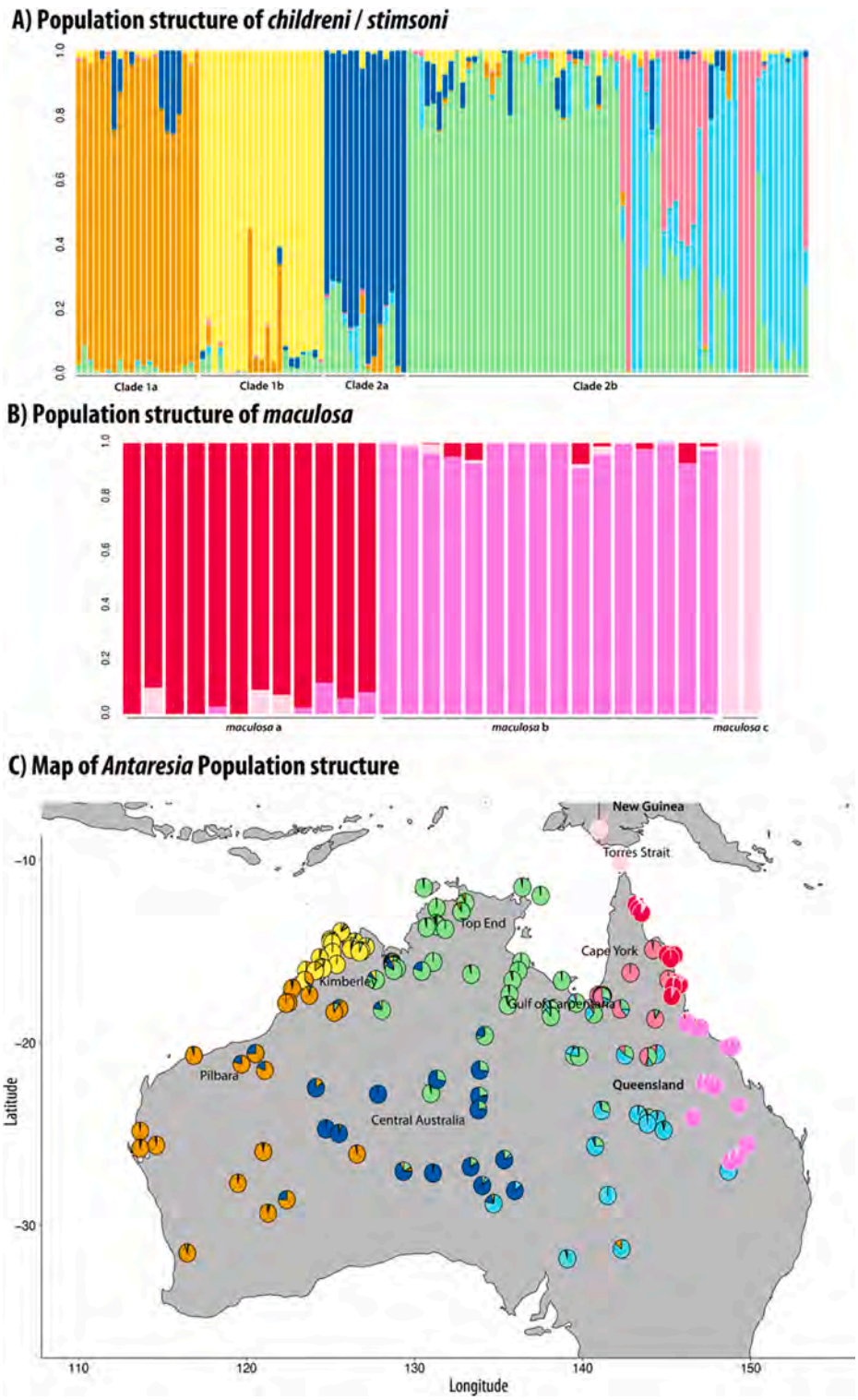

Fig. 3. **A**: Ancestry coefficient of each of the six identified genetic populations (K) for the *childreni / stimsoni* dataset, sorted by clade. **B**: Ancestry coefficient of each of the three identified genetic populations (K) for the *maculosa* dataset, sorted by clade. **C**: Distribution map of each of the specimens displayed as pie charts of their ancestry coefficients, to visualise the geographic effect of admixture. Samples from the *maculosa* dataset have a white outline.

maculosa a + b (Table 2). The northwest region of the Top End and northeast Kimberley is the probable origin of expansion for *childreni/stimsoni*, both when exploring the whole species or clade 2 alone (Fig. 7), expanding towards the south Kimberley/Top End. For *A. perthensis*, the origin of expansion is on northwest region of the species distribution, at the Mount Sheila region of Western Australia (Fig. 7). For *maculosa* a + b the southeast area of the clade distribution, in southeast Queensland, is the probable origin of expansion, expanding towards the north (Fig. 7).

3.6. Morphometrics

With the linear morphometrics of body shape and lepidosis we found a significant effect of clade, but not of sex or the interaction (clade $F(4, 205) = 194.24$, $P < 0.0001$; sex $F(1, 205) = 0.61$, $P = 0.5$; species*sex F

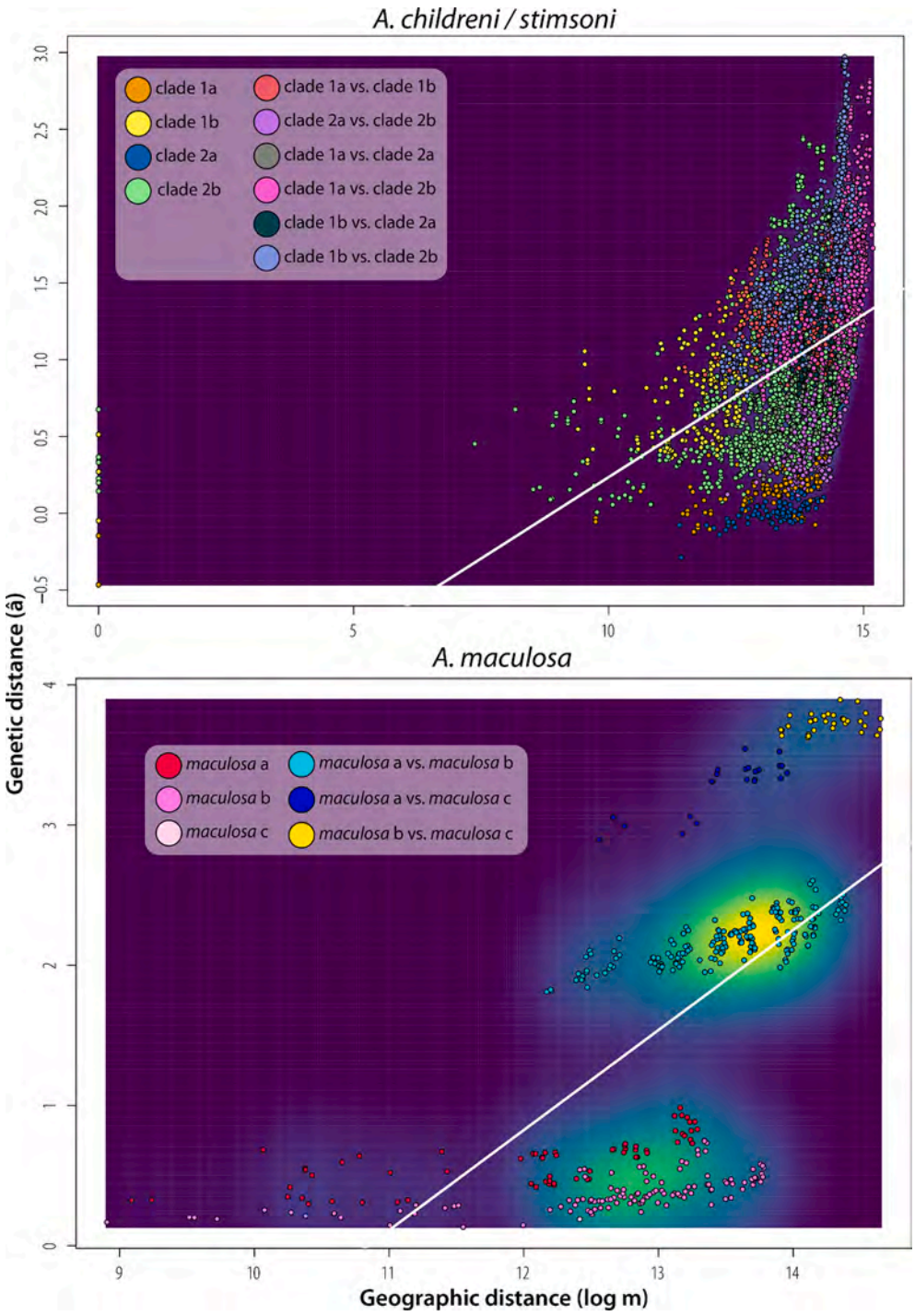

Fig. 4. Geographic vs genetic distance between samples of *A. childreni / stimsoni* (above) and *A. maculosa* (below). The background coloration corresponds to the kernel density of the distribution of the data.

(4, 205) = 0.59, P = 0.73), while with head shape we found a strong effect of clade and a weaker effect of sex, but no effect of the interaction of the terms (clade F(5, 196) = 11.08, P < 0.0001; sex F(1, 196) = 3.39, P = 0.01; species*sex F(5, 196) = 0.98, P = 0.459). The pairwise tests between clades revealed differences between the major clades, but not between subclades (Table S2). For the linear morphometrics, *maculosa* a was not significantly different from *childreni/stimsoni,* and *maculosa* c only had significative differences with *perthensis*, but this is likely a product of the lower power given fewer samples in *maculosa* a and c. Similarly, the PCA of linear measurements shows clear phenotypic differences between the main lineages (Fig. 8, Table S3). PC1 (27.33%) separates *childreni/stimsoni* with higher ventral, subcaudal, postoculars and loreals and thinner heads and necks on side, and *perthensis* with lower scale counts and wider heads and necks on the other, with *maculosa* being intermediate. PC2 (17.34%) mostly separates *maculosa* from the rest by having thicker and longer bodies and shorter heads and fewer loreal scales. *childreni/stimsoni* clade 1 tends to be further along PC1 than clade 2, but the *maculosa* clades largely overlap in their morphometrics. The PCA of head shape also separates major lineages but not subclades (Fig. 8). PC1 (48.84%) represents an elongation of the head and enlargement of the eyes, which shows that *childreni/stimsoni* tend to have thinner and elongated heads and proportionally larger eyes than

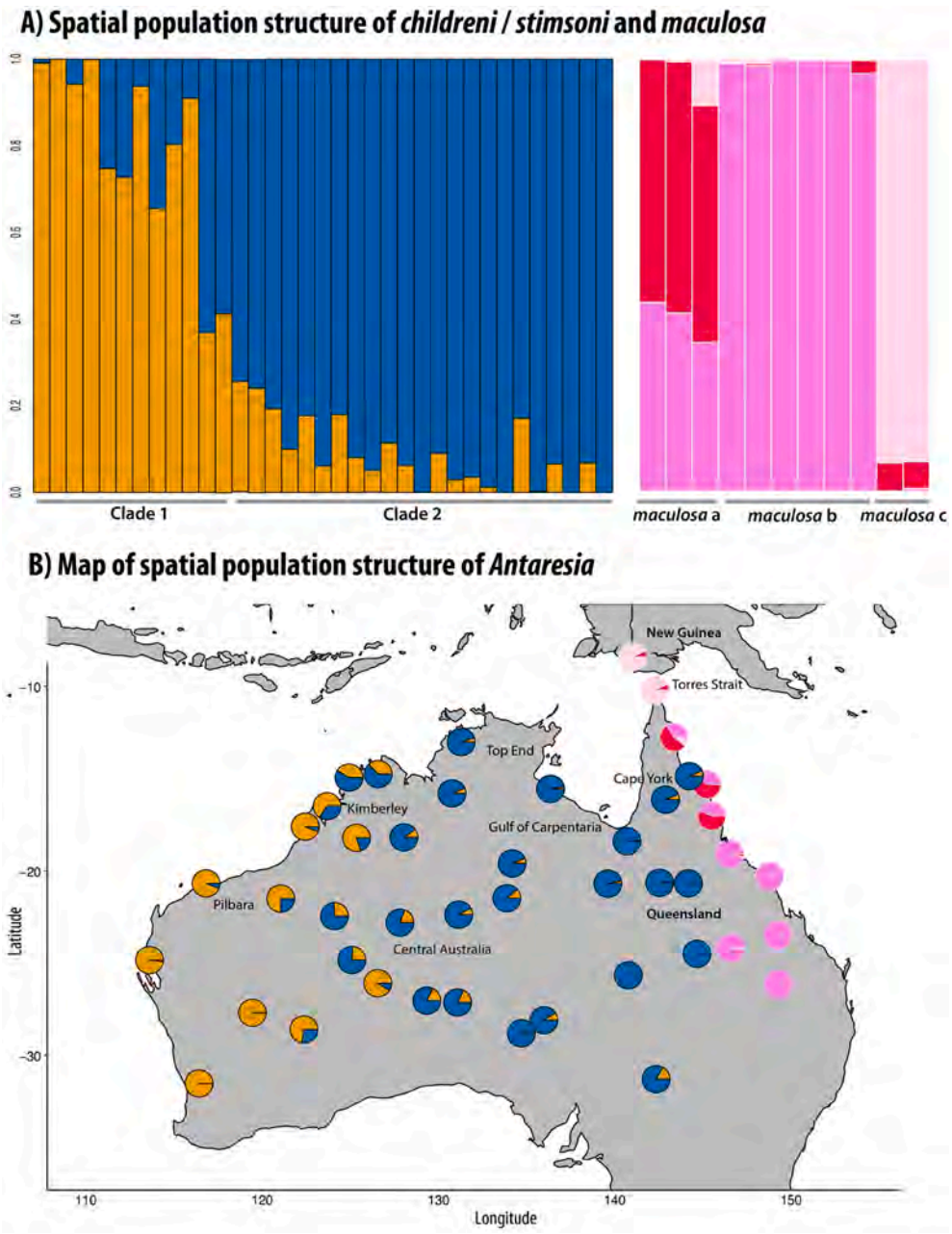

Fig. 5. **A**: Spatial ancestry coefficient for the samples of the *childreni/stimsoni* and *maculosa* datasets inferred by *conStruct*. **B**: Distribution map of each of the specimens displayed as pie charts of their ancestry coefficients, to visualise the geographic distribution of admixture. Samples from the *maculosa* dataset have a white outline.

Table 1
Fixed difference analysis results for the whole dataset. Upper triangle: count of loci showing fixed allelic differences between clades. Lower triangle: Expected number of false positives based on simulations. All comparisons were significant after simulation, with P values < 0.0001. The comparisons between *maculosa* clades come from the separate SNP dataset of that taxon.

	1	2	3	4	5
1. *childreni/stimsoni*	–	2694	2473	2763	792
2. *maculosa* a	96.6		168	497	2926
3. *maculosa* b	227.4	68.9	–	857	2741
4. *maculosa* c	41.8	198.8	164.6	–	3020
5. *perthensis*	75.8	193.4	296.2	131.2	–

maculosa, with *perthensis* being intermediate. PC2 (19.68%) represents a relative elongation of the snout (from eyes to tip of the snout) and tends to separate *maculosa* and *perthensis* on the negative end with shorter snouts than *childreni/stimsoni*. The remaining PCs in both analyses fail to separate the taxa, and are therefore irrelevant to this study.

A visualisation of variation in lepidosis across clades (Fig. S8 and Table S4) shows differences between major lineages (*perthensis*, *childreni/stimsoni* and *maculosa*), but very subtle or non-existing variation between subclades. *Antaresia perthensis* tend to have fewer ventral and subcaudal scales and heat pits in the infralabials than the rest, while *childreni/stimsoni* tend to have more ventral, supralabial, postocular and loreal scales than the rest. *Antaresia childreni/stimsoni* clade 1 tends to have higher scale counts than clade 2. *Antaresia maculosa* tend to have fewer loreal scales than the rest, and *maculosa* a tends to have more ventral scales than *maculosa* b. We also find that *maculosa* often has two

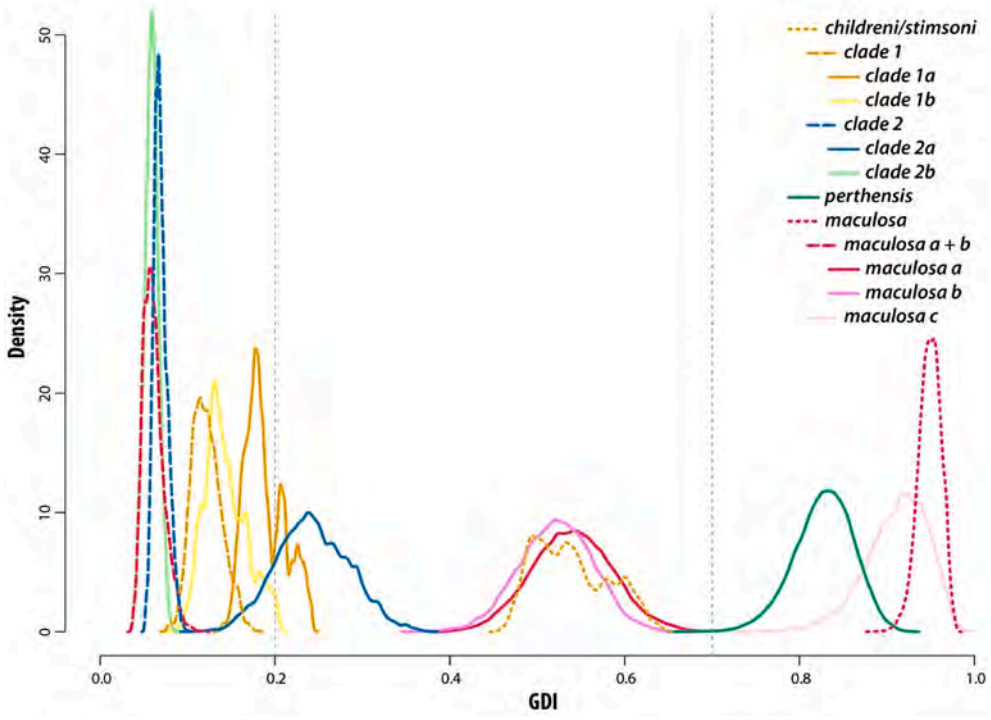

Fig. 6. Posterior densities of the genealogical divergence indexes (gdi) for the taxa/clades tested here.

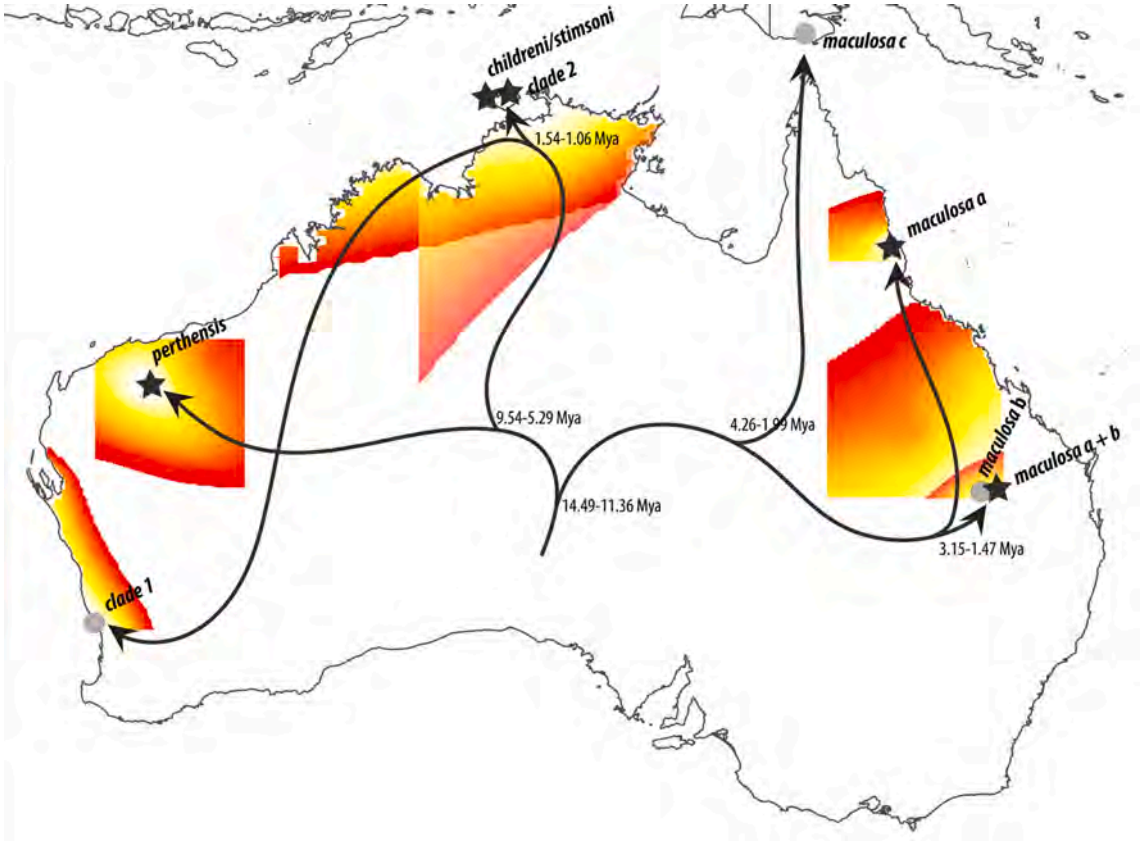

Fig. 7. Inferred origin by *rangeexpansion* for the main clades of *Antaresia*. Stars indicate clades where there is signal for significant range expansion and circles for clades there is not. Yellow and red shaded areas represent higher and lower probability of population origin, respectively. A tree is depicted on the map to illustrate the phylogenetic relationships between the clades with 95% HPD of node ages. (For interpretation of the references to colour in this figure legend, the reader is referred to the web version of this article.)

Table 2
Historical demography results, with number of samples (N), observed heterozygosity (Ho), Tajima's D, range expansion *P* values (bold ones statistically significant) and the Bonferroni corrected critical *P* values for the latter.

	N	Ho	Tajima's D	Expansion *P* value	Corrected critical *P* value
A. childreni/ stimsoni	124	0.011	−1.072	**9.16E-24**	0.00001
clade 1	42	0.007	−0.692	0.057	0.00006
clade 2	82	0.011	−1.093	**4.26E-12**	0.00002
A. perthensis	7	0.014	−0.204	**6.83E-10**	0.00238
A. maculosa	30	0.005	−0.503	0.079	0.00011
maculosa a + *maculosa* b	28	0.006	−0.503	**1.63E-22**	0.00013
maculosa a	12	0.008	−0.302	**3.92E-06**	0.00076
maculosa b	16	0.005	−1.069	0.013	0.00042

or three prefrontals, whereas the others always have four or more. Pattern and coloration are highly variable in all the lineages, in particular in *childreni/stimsoni*. We describe the variation in Table S4, and illustrate variation in Figs. 10 and 11.

4. Taxonomy

Based on the combined evidence from phylogenetics, genetic structure, species delimitation approaches and morphometrics we conclude that *Antaresia stimsoni* is not a biological lineage (Fig. 9). Even though there is some phylogeographic structure within the *childreni/stimsoni* clade, extensive gene flow, lack of nuclear loci showing fixed differences and lack of significant morphological differences leads us to formally relegate *A. stimsoni* to the status of a junior synonym of *A. childreni*.

There is some significant genetic structure found within *A. maculosa*, with the existence of three independent lineages with limited gene flow: *maculosa* a in Cape York, *maculosa* b in the rest of Queensland and *maculosa* c in New Guinea and Torres Strait (Fig. 9). Of the three, *maculosa* c is the most divergent, shows clear genetic isolation and is morphologically diagnosable, and we therefore describe it as a new species. The clades *maculosa* a and b are more closely related, and a lack of significant morphological differentiation and an apparent still early stage of genetic divergence dissuades us from describing them as full species. Instead, we describe these two clades as subspecies to account for the fact that they are at least in the incipient stages of speciation.

Antaresia maculosa maculosa

Liasis maculosus Peters 1873

Liasis maculosus Smith 1985

Morelia maculosa Underwood & Stimson 1990

Antaresia maculosa Kluge 1993

Antaresia maculosa Lawson, Slowinski & Burbrink 2004

Antaresia maculosa Rawlings, Rabosky, Donnellan & Hutchinson 2008

Antaresia maculosa Schleip & O'Shea 2010

Antaresia maculosa Barker, Barker, Davis & Schuett 2015

Antaresia maculosa Esquerré, Donnellan, Brennan, Lemmon, Lemmon, Zaher, Grazziotin & Keogh 2020

Lectotype. ZMB (Zoologisches Museum Berlin) 5984 collected at Port Mackay, Queensland, Australia (21.15°S; 149.18°E) by A. Dietrich.

Paralectotypes. ZMB 5890 collected at Rockhampton (23.37°S; 145°E) and ZMB 7513 collected at Port Bowen (=Port Clinton) (22.48°S; 150.75°E), Queensland, Australia, by A. Dietrich.

Diagnosis. The clade found in our analyses that we call *maculosa* b. It differs from *Antaresia perthensis* by having highly contrasted large dark blotches with usually ragged edges along the body (vs less contrasted blotches and dots), a larger body size (max. SVL 1220 mm vs 670 mm) and a higher number of ventrals (249–280 vs 213–247). It differs from *A. childreni* by having a blotched pattern (vs. being patternless) or by lacking a space between the blotches in the anterior third of the body creating a lateral pale stripe and by generally having more ragged edges on its blotches. There are no consistent morphological diagnostic characters to differentiate it from the subspecies in Cape York, but it can be differentiated from it by various nucleotide substitutions in the *cyt-b* gene (see Table S7). From the species in the Torres Strait and New Guinea it is differentiated by having larger and more contrasting blotches (vs smaller scattered dots), and by never having less than four prefrontal scales (vs. sometimes having two or three prefrontals).

Etymology. The subspecific name *maculosa* applies from being the nominotypical taxon *Antaresia maculosa*, which means 'spotted', hence we propose the common name 'Southern Spotted Python'.

Description. A small python, with a maximum recorded SVL of 1220 mm. Maximum recorded tail length is 112 mm and tail length is on average is 0.094 of the SVL. Head length is on average 0.036 of the SVL, and it is on average 1.68 times the head width. Maximum recorded mid-body girth is 140 mm, and it is on average 2.04 times thicker than the neck.

Head scalation comprises large symmetrical shields. One large roughly hexagonal or pentagonal frontal scale, divided into two scales longitudinally in some specimens. Two parietal scales directly in contact with the frontal, posterior to which scales are largely undifferentiated. Parietals usually in contact but sometimes small scales are formed between them or between them and the frontal. One large supraocular above each eye. Four large prefrontal scales, with sometimes one additional small scale between them. Two internasal scales. Rostral scale in contact with internasals, nasal and first supralabials. There are 9–12 supralabials with an average of 10.5; and 11–14 infralabials with an average of 12.9. Three to four of the infralabials have conspicuous heat pits. There is a single large, anteriorly pointed preocular scale, with an additional much smaller one between it and the fourth and/or fifth supralabial scales. There are 1–11 irregularly sized loreal scales. Two to four postocular scales. Dorsal scales are smooth, rhomboidal and slightly overlapping. In some cases, these are more elongated anteriorly and becoming more compact towards the tail. Ventral scales are transversally elongated shields; ranging in number from 249 to 280, with an average of 259.6. Anal scale is single (undivided). Subcaudal scales range from 37 to 46 with an average of 41.2, most of them divided but sometimes fused towards the tip of the tail.

Background colouration ranges between greyish brown, light sandy colour, and a more reddish ochre. The spots or blotches on top are much darker, ranging from chocolate brown to a reddish dark brown. Shape and distribution of the spots is very variable. They tend to have ragged edges and be irregular in shape. Spots sometimes fuse on the back, creating large continuous and irregular patches. Sometimes (e.g. specimens from Magnetic Island, Queensland), blotches are small and uniformly speckled along the body, and can be quite faint. There is a slightly iridescent sheen to the skin.

Natural History. A nocturnal and primarily terrestrial snake, although it can be seen climbing on shrubs and trees (Cogger, 2014). Found across a variety of habitats, including dry woodland, dry savanna and rainforest. Commonly found on or near rocky outcrops and sheltering in hollow logs, abandoned burrows, under rocks, in caves and under surface debris (Torr, 2000). The diet includes frogs, skinks, geckoes, small birds and rodents (Shine and Slip, 1990). In sites like the 'Bat Cleft' at Mt. Etna, Queensland, they have been observed aggregating around sites of *Miniopterus* spp. bat abundance to feed on them (Torr, 2000). In captivity, males have been observed to engage in combat, and be reluctant to feed in the presence of another male (Barker and Barker, 1994). Mating occurs between April and August. As in all Pythonidae, they are oviparous, with clutch size ranging from 4 to 19 eggs (Greer, 1997), that are laid between October and November, with an average incubation period of 52.6 days (Greer, 1997). As in most other pythons, females have been observed to brood their eggs (Barker and Barker, 1994), performing muscular contractions to maintain the egg temperature (Williams, 1992).

Distribution. Found in eastern Australia, at least as far north as the Paluma Range, north of Townsville, Queensland, and as far south as

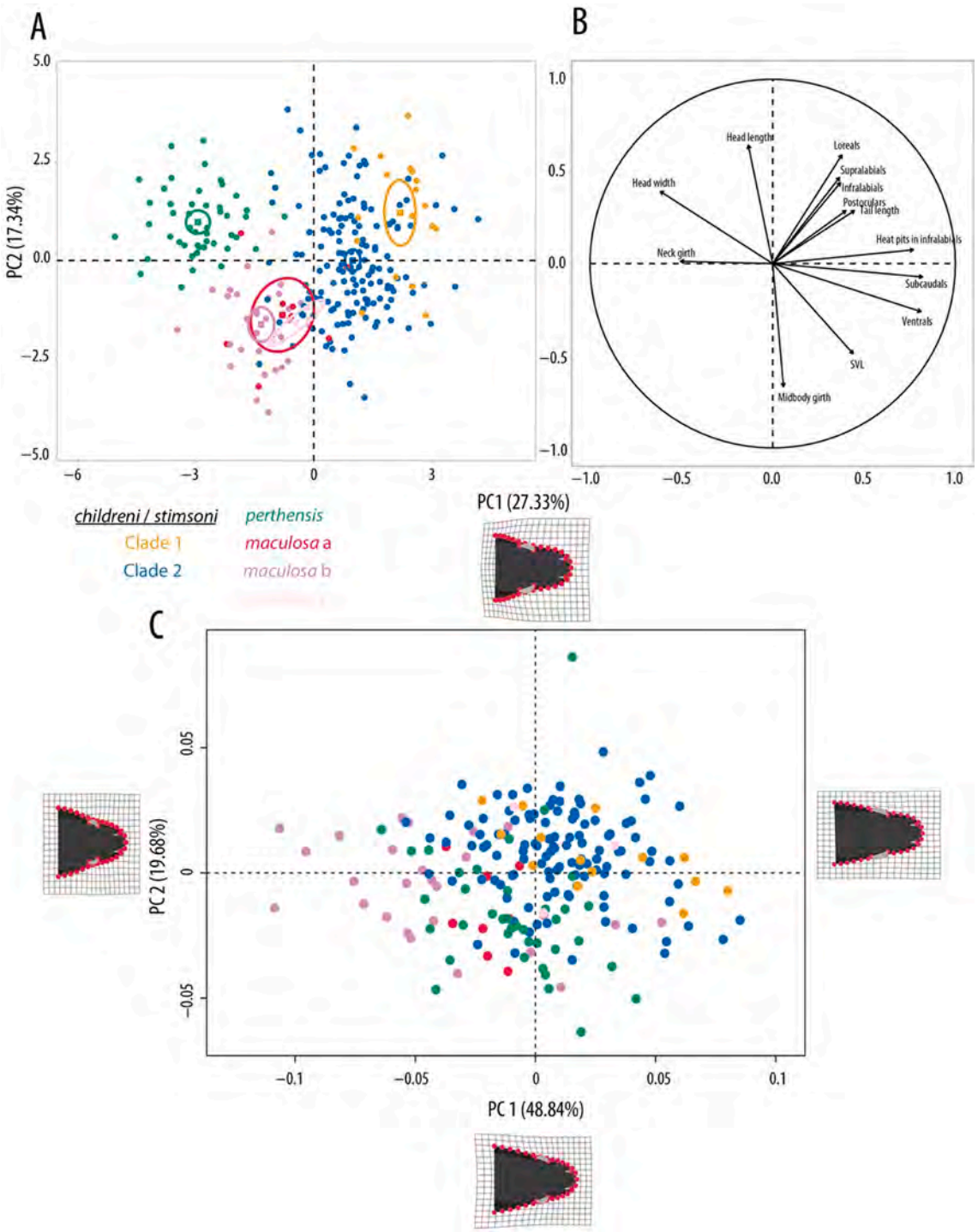

Fig. 8. **A**: Principal Component Analysis (PCA) plot for body shape and lepidosis, ellipses correspond to the 95% CI around the centroid of each species. **B**: Factor map illustrating the variable loadings for each PC. **C**: PCA of dorsal head shape, deformation grids illustrate the shape at the extreme of each axis.

north-eastern New South Wales (Cogger, 2014; Zozaya and Macdonald, 2013) (Fig. 1).

Antaresia maculosa peninsularis subsp. nov.

Liasis maculosus Peters 1873

Liasis maculosus Smith 1985

Morelia maculosa Underwood & Stimson 1990

Antaresia maculosa Kluge 1993

Antaresia maculosa Lawson, Slowinski & Burbrink 2004

Antaresia maculosa Rawlings, Rabosky, Donnellan & Hutchinson 2008

Antaresia maculosa Schleip & O'Shea 2010

Antaresia maculosa Barker, Barker, Davis & Schuett 2015

Antaresia maculosa Esquerré, Donnellan, Brennan, Lemmon, Lemmon, Zaher, Grazziotin & Keogh 2020

Holotype. SAMA R12797 (female), collected at Cooktown, Queensland, Australia (15.47°S; 142.25°E) by H. Ehmann in November 1971.

Paratypes. QMSB 33,588 (male) collected at Cairns area, Queensland (16.91°S; 145.77°E) in March 1975. QMSB 78,127 (sex unknown) collected at Lockhart River area, Queensland (12.97°S; 143.52°E) in July 2001. QMSB 31,830 (male) collected at Portland Roads,

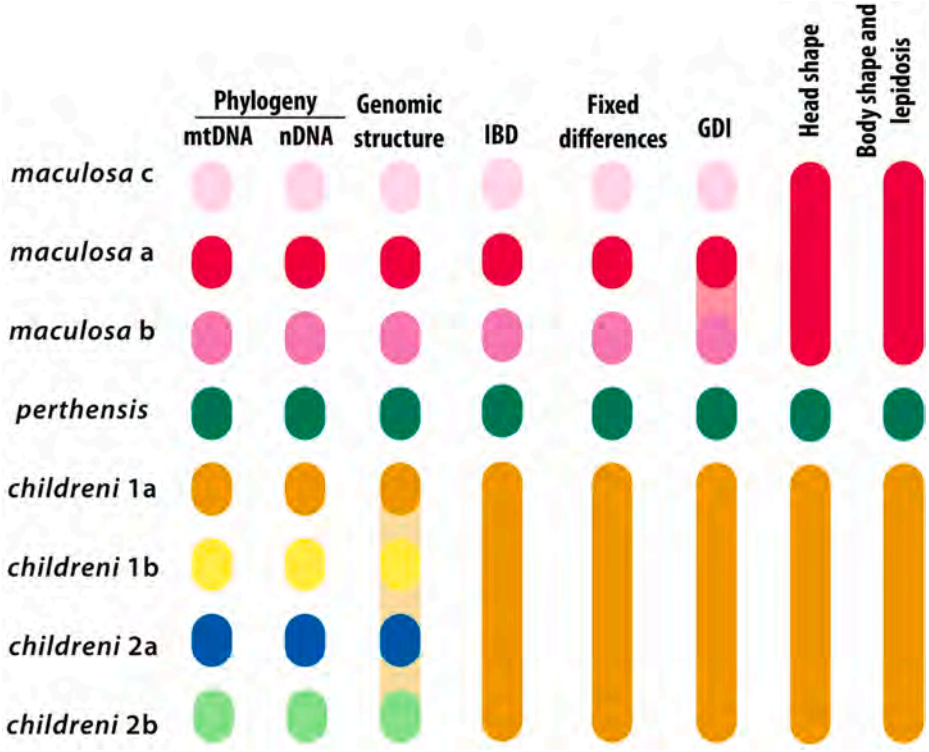

Fig. 9. Schematic showing the broad conclusions of the different lines of evidence of the integrative approach.

Queensland (12.6°S; 143.42°E) by G. Ingram on December 1978. MAGNT R5089 (male) collected at Edward River, Queensland (14.65°S; 142.05°E) by J. Bredl in 1976. SAMA R46757 (male) collected at Cairns, Queensland (16.92°S; 145.77°E) by R. Foster in January 1996. SAMA R4906 (female) collected at Cairns, Queensland (16.92°S; 145.77°E) by R. McKecknie in January 1963. SAMA R9942 (male) collected at Leggitts Lagoon, Queensland (15.43°S; 145.15°E) by F. Parker in May 1968.

Diagnosis. The clade found in our analyses that we call *maculosa* a. It differs from *Antaresia perthensis* by having highly contrasted large dark blotches with usually ragged edges along the body (vs less contrasted blotches and dots), a larger body size (max. SVL 1320 mm vs 670 mm) and a higher number of ventrals (252–287 vs 213–247). It differs from *A. childreni* by lacking a space between the blotches in the anterior third of the body creating a pale lateral stripe and by normally having more ragged edges on its blotches. There are no consistent morphological diagnostic characters to differentiate it from *A. maculosa maculosa*, but it can be differentiated from it by various nucleotide substitutions in the *cyt-b* gene (see Table S7). From the species in the Torres Strait and New Guinea it is differentiated by having larger and more contrasting blotches (vs smaller scattered dots), and by never having less than four prefrontal scales (vs sometimes having two or three prefrontals), and by never having less than three postocular scales (vs sometimes having two postoculars).

Description. Morphometric data of the type series can be found in Table S5. A small python, with a maximum SVL of 1320 mm. Maximum tail length (TL) is 110 mm, average TL/SVL is 0.096. Average HL/SVL is 0.035, average HL/HW is 1.75. Maximum mid-body girth is 115 mm, and it is on average 1.75 times thicker than the neck.

Head scalation comprises large symmetrical shields. One large roughly hexagonal frontal scale. Two parietal scales directly in contact with the frontal, posterior to which scales are largely undifferentiated. Parietals usually in contact but sometimes small scales are formed between them or between them and the frontal. One large supraocular above each eye. Four large prefrontal scales, with sometimes one additional small scale between them. Two internasal scales. Rostral scale in contact with internasals, nasal and first supralabials. There are 9–12 supralabials with an average of 10.5; and 12–14 infralabials with an average of 13.3. Three to four of the infralabials have conspicuous heat pits. There is a single large, anteriorly pointed preocular scale, with sometimes an additional much smaller one between this and the fourth and/or fifth supralabial scales. There are 3–7 irregularly sized loreal scales. Three to four postocular scales. Dorsal scales are smooth, rhomboidal and slightly overlapping. In some cases, these are more elongated anteriorly and becoming more compact towards the tail. Ventral scales are transversally elongated shields; they range from 252 to 287, with an average of 271.4. Anal scale is single (undivided). Subcaudal scales range from 40 to 48 with an average of 43.6, most of them divided but sometimes fused towards the tip of the tail.

Background colouration ranges between greyish brown, light sandy colour, and a more reddish ochre. The spots or blotches on top are much darker, ranging from chocolate brown to a reddish dark brown. Shape and distribution of the spots is very variable. They tend to have ragged edges and be irregular in shape. They sometimes fuse on the back, creating large continuous and irregular patches. There is a slightly iridescent sheen to the skin.

Natural History. A nocturnal and primarily terrestrial snake, whose ecology is undocumented but should be similar to the nominal subspecies (see above).

Distribution. Found in the northeast of Australia, mostly in the Cape York Peninsula, at least between Kutini-Payamu (Iron Range) National Park and the south of Cairns (Fig. 1). Populations on the far north of Cape York Peninsula need further assessment.

Etymology. The Latin name *peninsularis* refers to the Cape York Peninsula, where this taxon is found. We propose the common name 'Cape York Spotted Python' for this subspecies.

Antaresia papuensis sp. nov.

Antaresia maculosa O'Shea, Sprackland & Bigilale 2004

Antaresia maculosa Natusch & Lyons 2011

Holotype. AMS (Australian Museum, Sydney) 58,998 (male) collected at Badu Island, Torres Strait, Queensland (10.12°S; 142.12°E) by H. Heatwole in December 1976.

Paratypes. PNGM (Papua New Guinea National Museum and Art

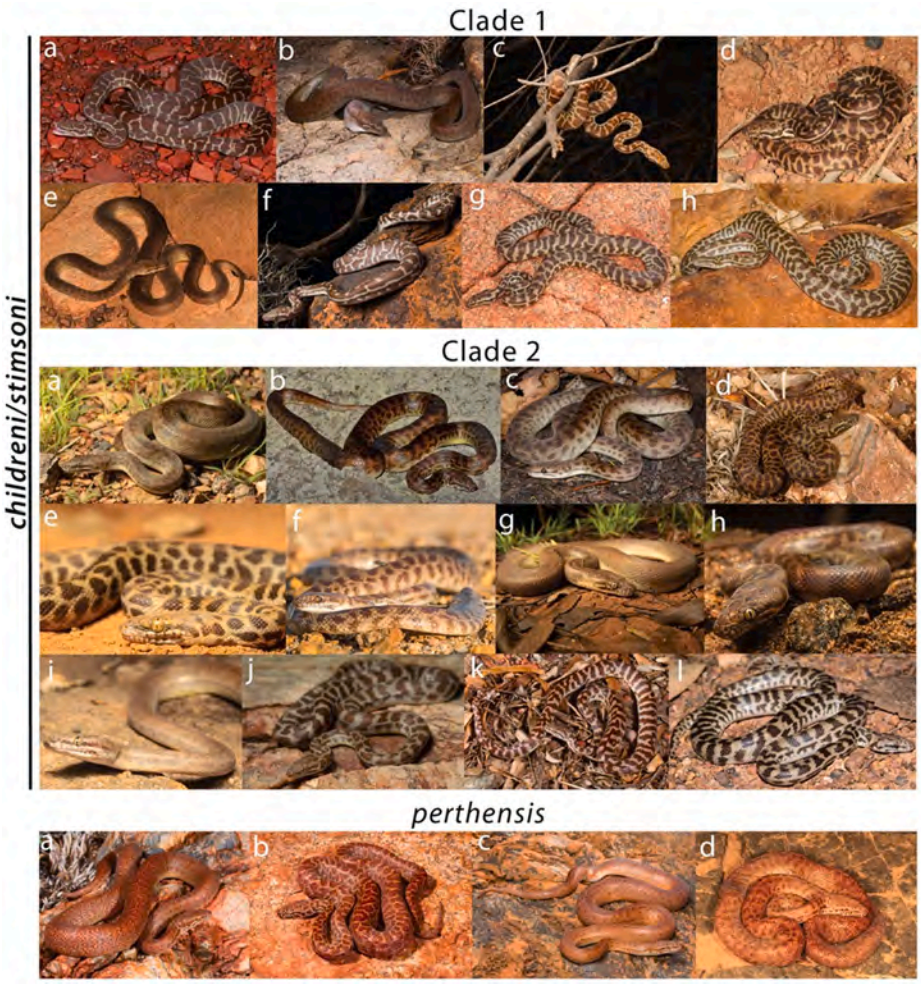

Fig. 10. A sample of the colour and pattern variation across *Antaresia childreni/stimsoni* and *perthensis*. Clade 1. a) Karijini National Park, Western Australia (Stephen Zozaya). b) Theda Station, Western Australia. (Stephen Zozaya). c) Near Broome, Western Australia. (Eric Vanderduys). d) Kalbarri National Park, Western Australia (Ryan Ellis). e) Drysdale River National Park, Western Australia (Ryan Ellis). f) Lake Barlee, Western Australia (Jari Cornelis). g) Indee Station, Western Australia (Ryan Ellis). h) Hamelin Station, Western Australia (Damian Lettoof). Clade 2. a) Near Adelaide River, Northern Territory (Damien Esquerré). b) Fogg Dam, Northern Territory (Damian Lettoof). c) Cooinda, Northern Territory (Chris Jolly). d) Top Springs, Northern Territory (Chris Jolly). e) Gundabooka National Park, New South Wales (Damien Esquerré). f) Croydon, Queensland (Damien Esquerré). g) Limmen National Park, Northern Territory (Damien Esquerré). h) Mary River National Park, Northern Territory. (Damien Esquerré). i) Kakadu National Park, Northern Territory (Damien Esquerré). j) West MacDonnell National Park, Northern Territory (Damien Esquerré). k) Mount Carbine, Queensland (Stephen Zozaya). l) Laura, Queensland (Justin Wright). *perthensis*. a) Marble Bar, Western Australia (Stephen Zozaya). b) Indee Station, Western Australia (Stephen Zozaya). c) Hamersley Range, Western Australia (Damian Lettoof). b) Warrawagine Station, Western Australia (Ryan Ellis).

Gallery) 25,085 collected at Weam, Western Province, Papua New Guinea (8.61°S; 141.12°E) by M. O'Shea in August 2000. AMS R47895 (female) collected at Hammond Island, Torres Strait, Queensland (10.53°S; 142.22°E) by P. Webber in March 1975. AMS R46906 and AMS R47383 collected at Moa Island, Torres Strait, Queensland (10.18°S; 142.27°E) by P. Webber, Cameron and Young in February 1975.

Diagnosis. The clade found in our analyses that we call *maculosa* c. It differs from *Antaresia perthensis* by a larger body size (max. SVL 1080 mm vs 670 mm) and a higher number of ventrals (253–284 vs 213–247). It differs from *A. childreni* by lacking a space between the blotches in the anterior third of the body creating a pale stripe and by normally having more ragged edges on its blotches. It differs from *A. m. maculosa* and *A. m. peninsularis* by having a far less contrasted pattern (vs a pattern of large contrasted blotches), with small scattered spots rather than large and dark irregular blotches. It also sometimes displays two or three prefontal scales (vs always four or more). It additionally differs from *A. m. peninsularis* by sometimes having two postocular scales (vs always three or four).

Description. Morphometric data of the type series can be found in Table S6. A small python, with a maximum recorded SVL of 1080 mm. Maximum tail length (TL) is 95 mm, average TL/SVL is 0.094. Average HL/SVL is 0.038, average HL/HW is 1.94. Maximum mid-body girth is 85 mm, and it is on average 1.72 times thicker than the neck.

Head scalation comprises large symmetrical shields. One large roughly hexagonal frontal scale. Two parietal scales directly in contact with the frontal, posterior to which scales are largely undifferentiated. Parietals in contact. One large supraocular above each eye. Two to four large prefrontal scales. Two internasal scales. Rostral scale in contact with internasals, nasal and first supralabials. There are 10–12 supralabials with an average of 10.6; and 10–14 infralabials with an average of 12. Four of the infralabials have conspicuous heat pits. There is a single large, anteriorly pointed preocular scale, with sometimes an additional much smaller one between this and the fourth and/or fifth supralabial scales. There are 3–5 irregularly sized loreal scales. Two to four postocular scales. Dorsal scales are smooth, rhomboidal and slightly overlapping. In some cases, these are more elongated anteriorly and becoming more compact towards the tail. Ventral scales are transversally elongated shields; they range from 253 to 284, with an average of 270.6. Anal scale is single (undivided). Subcaudal scales range from 40 to 48 with an average of 42.8, most of them divided but sometimes fused towards the tip of the tail.

Background colouration ranges between light to dark brown. There are small and irregular dark brown blotches along the dorsal surface, with ragged edges. There is a slightly iridescent sheen to the skin.

Natural History. It is likely this taxon displays a very similar ecology to *Antaresia maculosa*. Very little has been documented on *A. papuensis*. They are nocturnal (Natusch and Lyons, 2011) and shelter during the day, like a specimen that was found under corrugated iron (O'Shea et al., 2004). It has been reported that this species has been harvested from the wild for the international pet trade (Natusch and Lyons, 2011).

Distribution. Very few specimens have been recorded by science. In New Guinea, this species has been found in Weam, Western Province, Papua New Guinea (O'Shea et al., 2004) and Sota, West Papua, Indonesia (Natusch and Lyons, 2011). It is possible the species is widespread across the Trans-Fly region of New Guinea. In the Torres

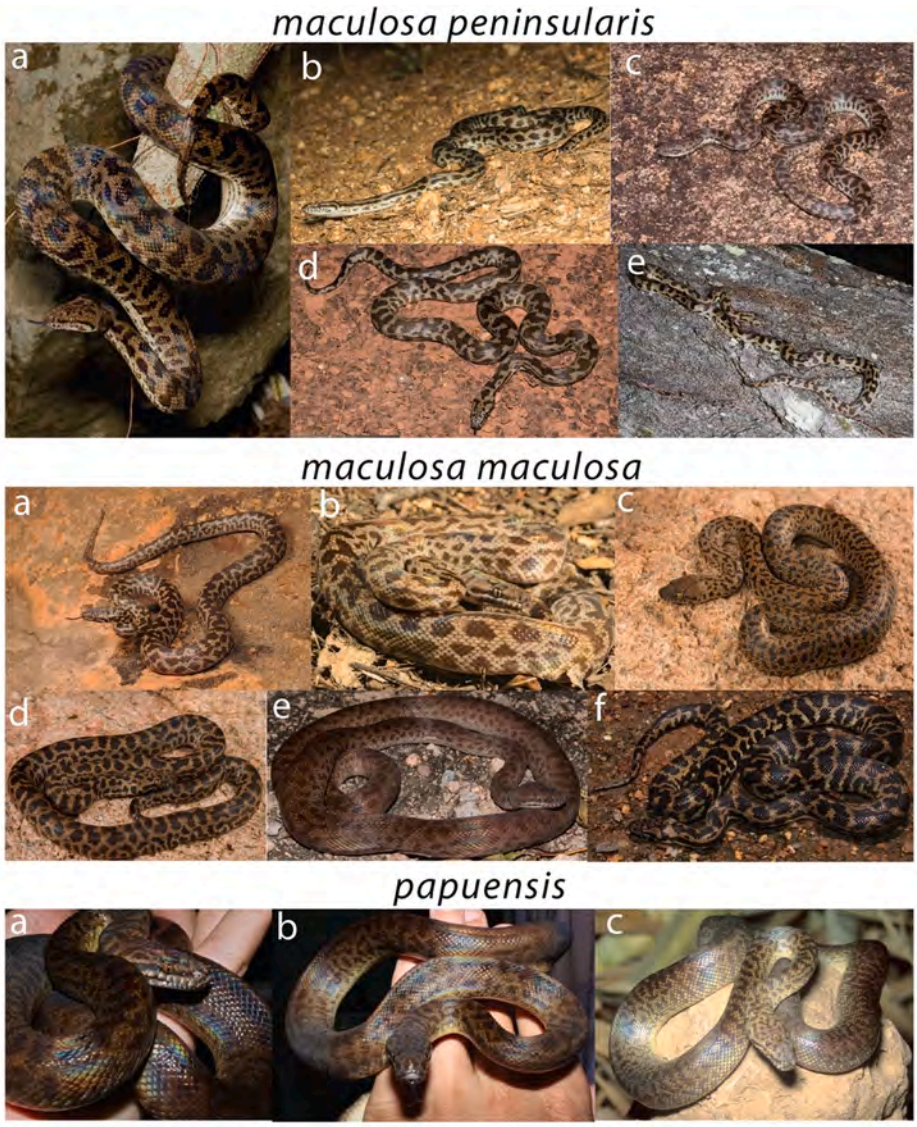

Fig. 11. A sample of colour and pattern variation across *Antaresia maculosa* and *papuensis*. *maculosa peninsularis*. a) Cairns, Queensland (Damian Lettoof). b) Iron Range National Park, Queensland (Damien Esquerré). c) Undara, Queensland (Stephen Zozaya). d) Weipa, Queensland (Justin Wright). e) Brooklyn, Queensland (Eric Vanderduys). *maculosa maculosa*. a) Just Range, Queensland (Eric Vanderduys). b) Townsville, Queensland (Damien Esquerré). c and d) Juveniles from Townsville, Queensland (Justin Wright). e) Magnetic Island, Queensland (Justin Wright). f) Charters Towers, Queensland (Justin Wright). *papuensis*. a and b) Sota, Papua, Indonesia (Daniel Natusch). c) Weam, Western Province, Papua New Guinea (Mark O'Shea).

Strait, this taxon has been found on Badu, Hammond, Moa and Saibai Islands. Specimens from the far north end of Cape York reportedly look more similar to *papuensis* than *peninsularis* (D. Natusch, pers. com.), but a genetic assessment is needed to confirm the identify of those populations.

Etymology. The Latin name *papuensis* derives from Papua, one of the names given to the island of New Guinea, where this taxon is found. We suggest 'Papuan Spotted Python' as a common name.

5. Discussion

Since their origin around the mid Miocene (Esquerré et al., 2020), two main lineages of *Antaresia* have undergone very different evolutionary trajectories. On one hand, we observe that the morphologically variable *Antaresia childreni / A. stimsoni* clade, widely distributed throughout most of the Australian continent, comprises a young network of genetically connected populations where the observed phenotypic variation does not reflect evolutionary history. On the other hand, we unexpectedly found significant genetic structure suggesting some degree of reproductive isolation among three morphologically conservative clades of *A. maculosa*, enough to warrant the recognition of a new species (*A. papuensis*) and two subspecies (*A. m. maculosa* and *A. m. peninsularis*). We discuss the implications of our findings in the context of biogeography, species delimitation and systematics.

5.1. Phylogenetics and systematics

Smith (1985), based on colour pattern, proposed two groups for the species now included in *Antaresia*: one with persistent patterning (*A. stimsoni* and *A. maculosa*) and one without persistent patterning (*A. childreni* and *A. perthensis*). Later, phylogenetic studies based on morphological characters failed to provide a robust hypothesis for the relationships between these species (Kluge, 1993; Underwood and Stimson, 1990). However, our study strongly supports the conclusions from phylogenetic analyses of other molecular genetic datasets (Esquerré et al., 2020, 2017; Pyron et al., 2013; Rawlings et al., 2008; Reynolds et al., 2014) that *Antaresia maculosa* is the sister taxon to the rest of the genus and *A. perthensis* is the sister of *A. childreni*. The novel finding of our study is the revelation of levels of genetic differentiation and isolation among clades and populations of this genus of pythons that contrast markedly with existing taxonomic boundaries.

Antaresia childreni was considered a distinct species from *A. stimsoni,* separated in a north/south fashion, with the former taxon across Australia's Top End and the latter widespread throughout the southern more arid zones. This was mostly based on the fact that there is a tendency for lack of pattern around the monsoonal tropics in the Top End and an

increase in contrasted pattern towards more arid zones. Additionally, *A. stimsoni* comprised two subspecies: *A. s. stimsoni* in western Western Australia and *A. s. orientalis* in the rest of the distribution. We find no evidence for this arrangement. Instead, we infer two clades both comprising populations of northern patternless '*A. childreni*' and southern patterned '*A. stimsoni*', which are separated east and west, rather than north and south. Our population structure and species delimitation analyses demonstrate that these clades have considerable admixture near the contact zones and lack loci with fixed allelic differences. Thus, lack of support for genetic isolation indicates that there is little reason to believe these two clades are at any detectable stage of speciation, and we now consider them a widespread and morphologically variable single species (see Fig. 10). This makes *A. childreni* one of the most widely distributed snakes in Australia. It remains an interesting question if this pattern variation between arid and monsoonal areas is linked to particular selective pressures related to the diverse environments these snakes live in.

Antaresia maculosa offers a contrasting pattern. Although reasonably variable in pattern (Fig. 11), geographic structuring of morphological variation is not evident and the only obvious geographical feature that could act as reproductive barrier is the Torres Strait. Thus, previous research has largely ignored the divergence between populations. We find strong support for three well-structured clades, one in New Guinea and Torres Strait, one in Cape York and one in central to southern Queensland. Although some limited admixture exists near the contact zones, in particular between the two Australian clades, we provide strong evidence for very restricted gene flow. The combined body of evidence does point to two distinct but recently diverged lineages (*A. maculosa* and *A. papuensis*), and a pair of lineages in the early stages of speciation (*A. m. maculosa* and *A. m. peninsularis*). We acknowledge that the two subspecies of *A. maculosa* are for the moment very hard to diagnose in the field, and that it will be hard to assign specimens from intermediate localities we haven't included in this study. A future study should include a denser sampling, especially around contact zones, to delimit the precise geographic distributions of the two or potentially reveal gene flow or less genetic differentiation between *A. m. maculosa* and *A. m. peninsularis*.

5.2. The idiosyncratic trajectories of different lineages of Antaresia

Antaresia likely originated within the Australian continent sometime in the mid to late Miocene (Esquerré et al., 2020). *A. maculosa* was restricted to eastern Australia and particularly associated with the more humid tropical regions of Queensland. After the early divergence of *A. papuensis* in the Pliocene, which either dispersed into New Guinea possibly through one of the Plio-Pleistocene land bridges (Chivas et al., 2001; Macqueen et al., 2010; Voris, 2000; Yokoyama et al., 2001) or experienced vicariance from Australian populations, its sister lineage later diverged into *A. m. maculosa* and *A. m. peninsularis*, expanding in range from southern Queensland towards the north. The level of genetic structuring, small population sizes and a positive sign for range expansion in *peninsularis* suggest this clade was isolated from the southern *maculosa*, possibly through range contractions, and subsequently expanded, getting into secondary contact at the base of Cape York. This offers an interesting contrast with the green tree python (*Morelia viridis*), where populations from Cape York and southern New Guinea display no divergence (Natusch et al., 2020).

The sister lineage to *A. maculosa* and *A. papuensis* diverged into *A. perthensis* and *A. childreni* likely in the late Miocene, with the former becoming isolated in the arid zones of the Pilbara and surroundings. The elevated H_o and near zero Tajima's D of *A. perthensis* suggest large effective population sizes and greater stability, possibly product of this taxon's persistence in the Pilbara. *A. childreni* spread towards most of Australia's warm regions, both arid and wet, maintaining large populations. This species originated or had refugia in the Top End or Kimberley, one of Australia's biodiversity hotspots (Bowman et al., 2010; Moritz et al., 2013) where many vertebrate lineages have originated (Potter et al., 2016). Despite its large range and morphological variability, *Antaresia childreni* appears to be the youngest taxon of *Antaresia*, with a crown age estimated in the Pleistocene. We also find that *A. childreni* has significantly greater ancestral population sizes than those of *A. maculosa* and *A. perthensis*, and it is well understood that speciation times are negatively correlated with population sizes (Gavrilets et al., 2000; Orr and Orr, 1996; Rannala and Yang, 2003). Additionally, the high degree of habitat generalism of this species (Greer, 1997; Torr, 2000) suggests that there are few geographical barriers to migration between populations. Some degree of population structure within a wide-spread species, as observed in *A. childreni*, is not surprising (Coates et al., 2018), but the large population sizes and ranges preclude them from diverging into independent evolutionary entities. *Antaresia maculosa* has much smaller ancestral population sizes, which could have led to accelerated rates of genetic divergence.

5.3. The Papuan Spotted python

Antaresia was first recorded in New Guinea from a single specimen collected in Papua New Guinea in 2004 (O'Shea et al., 2004), and since then only a handful of specimens have been reported from across the border in Papua, Indonesia (Natusch and Lyons, 2011). Our study indicates that the populations there and in Torres Strait are divergent from Australian populations, and we describe them as a separate species. However, unlike spotted pythons in Australia, very little is known about the distribution, ecology and conservation status of *A. papuensis*. We simply have no data as to whether they are found across all southern New Guinea's tropical woodlands or even north of the central mountain range, which is known to act as an allopatric barrier for pythons and other lowland taxa (Natusch et al., 2020; Rawlings and Donnellan, 2003). The presence of *A. papuensis* in the Australian mainland is also plausible, as specimens from the tip of Cape York resemble those of *A. papuensis* (Natusch, pers. com.). Further genetic analysis of these populations and conducting surveys in New Guinea is important, as the New Guinean populations are harvested from the wild (Natusch and Lyons, 2011).

5.4. The challenge of species delimitation at shallow scales

Often studies present phylogenies where well supported clades are provided as evidence for independently evolving lineages (i.e. species) (Kvist, 2013; Moritz and Cicero, 2004). More recently, many researchers are applying species delimitation methods based on the MSC to infer species boundaries, despite the tendency of these methods to overestimate species-level diversity (Jackson et al., 2017; Leaché et al., 2018; Sukumaran and Knowles, 2017). If we had taken either approach, rather than relying on an integrative framework, we could have recognised up to nine species. Inflating our estimates of biodiversity can create more problems than it solves, in particular for conservation management and studies on ecology and evolution (Isaac et al., 2004). It might not yet be realistic to produce large genomic scale datasets for every group needing systematic revision, but an assessment of gene and genetic isolation between detected lineages is central to accurately delimiting taxa. Fortunately, genome complexity reduction techniques, such as the one used here, are more accessible and provide good value for the amount and quality of data produced (Harvey et al., 2016; Leaché and Oaks, 2017). These methods are now being used for a number of different vertebrate groups (e.g. Chaplin et al., 2019; Esquerré et al., 2019; Georges et al., 2018; Mahony et al., 2020; Oliver et al., 2020; Potter et al., 2016).

Evolutionary biologists have been long moving away from a view of species as discrete entities (Mallet, 2008). As speciation is a protracted process, when we deal with these 'gray zones' of speciation (Coates et al., 2018; Singhal et al., 2018), subjectivity is impossible to avoid (Georges et al., 2018; Sites and Marshall, 2004). This provides a

challenge when trying to translate the subtleties and complexities of evolution into binomial nomenclature. We argue that infraspecific taxonomic categories such as subspecies, as we applied for *Antaresia maculosa*, are of great utility to acknowledge the early stages of speciation into formal descriptions of diversity (Mulcahy, 2008), that then facilitate the inclusion of appropriate levels of biological diversity in formal conservation legislative frameworks (Hillis, 2019).

Closing remarks

Our study adds to the rapidly growing number of studies showing how genome-wide sequencing techniques can vastly improve our understanding of the evolutionary history of a group (e.g. Chaplin et al., 2019; Spinks et al., 2014). The rise of next generation sequencing now calls for a general reassessing of biodiversity and species boundaries, particularly in this age of mass extinction. We show how using these sorts of data extract an astounding amount of information about the evolution of a group, ranging from phylogenetic relationships and lineage delimitation, to assessing population fluctuations, range expansions and gene flow, which combined can give us a clearer picture of the processes that shape biodiversity.

Author contributions

DE, SD and JSK conceived and designed the project; DE collected the data; DE, CJP and JF analysed the data and all authors contributed to interpretation of the results; DE and CJP prepared the figures; DE wrote the initial draft and all authors contributed to editing and improving it.

Declaration of Competing Interest

The authors declare that they have no known competing financial interests or personal relationships that could have appeared to influence the work reported in this paper.

Acknowledgements

We thank Sarah Catalano for performing most of the mitochondrial sequencing. We thank Graeme Armstrong, Jan Armstrong, Gavin Bedford, Ian Brennan, Peter Birch, Paul Doughty, Harald Ehmann, Ryan Ellis, Ralph Foster, Graeme Gillespie, Mark Hutchinson, Steve McAlpin, Craig Moritz, Dan Natusch, Dave Pearson, Luke Price, Lesley Rawlings, Anthony Stimson and Dane Trembath for tissues. We thank Jari Cornelis, Ryan Ellis, Chris Jolly, Damian Lettoof, Dan Natusch, Mark O'Shea, Eric Vanderduys, Justin Wright and Stephen Zozaya for providing photos of *Antaresia*. We thank Jodi Rowley and Dane Trembath from the Australian Museum for facilitating access to the type series of *Antaresia papuensis*. We thank Ziheng Yang and Adam Leaché for help with BPP and Renee Catullo for help with the population structure analyses. Mitochondrial sequencing was supported by funding from Craig Moritz's ARC Linkage Project grant LP120200063 and the SNP data collection was funded by an ARC Discovery grant to Scott Keogh and Steve Donnellan (DP120104146). Finally, we thank two reviewers whose comments helped improve the manuscript.

Appendix A. Supplementary data

Supplementary data to this article can be found online at https://doi.org/10.1016/j.ympev.2021.107181.

References

Adams, D.C., Collyer, M.L., Kaliontzopoulou, A., Sherratt, E., 2016. Geomorph (Version 3.0.2,): Geometric morphometric analyses of 2D/3D landmark data.

Angelis, K., Reis, dos M., 2015. The impact of ancestral population size and incomplete lineage sorting on Bayesian estimation of species divergence times. Curr. Zool. 61, 874–885. https://doi.org/10.1093/czoolo/61.5.874.

Barker, D.G., Barker, T.M., 1994. Pythons of the world. Volume I, Australia. Lakeside, CA, USA.

Barker, D.G., Barker, T.M., Davis, M.A., Schuett, G.W., 2015. A review of the systematics and taxonomy of Pythonidae: an ancient serpent lineage. Zool. J. Linnean Soc. 175, 1–19. https://doi.org/10.1111/zoj.12267.

Barley, A.J., Nieto Montes de Oca, A., Reeder, T.W., Manríquez-Morán, N.L., Hernández-Gallegos, O., Thomson, R.C., 2019. Complex patterns of hybridization and introgression across evolutionary timescales in Mexican whiptail lizards (*Aspidoscelis*). Mol. Phylogenet. Evol. 132, 284–295. https://doi.org/10.1016/j.ympev.2018.12.016.

Bowman, D.M.J.S., Brown, G.K., Braby, M.F., Brown, J.R., Cook, L.G., Crisp, M.D., Ford, F., Haberle, S., Hughes, J., Isagi, Y., Joseph, L., McBride, J., Nelson, G., Ladiges, P.Y., 2010. Biogeography of the Australian monsoon tropics. J. Biogeogr. 37, 201–216. https://doi.org/10.1111/j.1365-2699.2009.02210.x.

Bradburd, G.S., Coop, G.M., Ralph, P.L., 2018. Inferring continuous and discrete population genetic structure across space. Genetics 210, 33–52. https://doi.org/10.1534/genetics.118.301333.

Chaplin, K., Sumner, J., Hipsley, C.A., Melville, J., 2019. An integrative approach using phylogenomics and high-resolution X-ray computed tomography for species delimitation in cryptic taxa. Syst. Biol. 98, 1049–1114. https://doi.org/10.1093/sysbio/syz048.

Chernomor, O., von Haeseler, A., Minh, B.Q., 2016. Terrace aware data structure for phylogenomic inference from supermatrices. Syst. Biol. 65, 997–1008. https://doi.org/10.1093/sysbio/syw037.

Chifman, J., Kubatko, L., 2014. Quartet inference from SNP data under the coalescent model. Bioinformatics 30, 3317–3324. https://doi.org/10.1093/bioinformatics/btu530.

Chivas, A.R., García, A., van der Kaars, S., Couapel, M.J.J., Holt, S., Reeves, J.M., Wheeler, D.J., Switzer, A.D., Murray-Wallace, C.V., Banerjee, D., Price, D.M., Wang, S.X., Pearson, G., Edgar, N.T., Beaufort, L., De Deckker, P., Lawson, E., Cecil, C.B., 2001. Sea-level and environmental changes since the last interglacial in the Gulf of Carpentaria, Australia: an overview. Quat. Int. 83-85, 19–46. https://doi.org/10.1016/S1040-6182(01)00029-5.

Claude, J., 2013. Log-shape ratios, Procrustes superimposition, elliptic Fourier analysis: three worked examples in R. Hystrix 24, 94–102. https://doi.org/10.4404/hystrix-24.1-6316.

Coates, D.J., Byrne, M., Moritz, C., 2018. Genetic diversity and conservation units: dealing with the species-population continuum in the age of genomics. Front. Ecol. Evol. 6, 4045–4113. https://doi.org/10.3389/fevo.2018.00165.

Cogger, H.G., 2014. Reptiles and amphibians of Australia, seventh ed. Collingwood, Australia.

Collyer, M.L., Adams, D.C., 2018. RRPP: An R package for fitting linear models to high-dimensional data using residual randomization. Methods Ecol. Evol. 9, 1772–1779. https://doi.org/10.1111/2041-210X.13029.

Dayrat, B., 2005. Towards integrative taxonomy. Biol. J. Linnean Soc. 85, 407–417. https://doi.org/10.1111/j.1095-8312.2005.00503.x.

De Queiroz, K., 2007. Species concepts and species delimitation. Syst. Biol. 56, 879–886. https://doi.org/10.1080/10635150701701083.

Devitt, T.J., Wright, A.M., Cannatella, D.C., Hillis, D.M., 2019. Species delimitation in endangered groundwater salamanders: Implications for aquifer management and biodiversity conservation. Proc. Natl. Acad. Sci. U.S.A. 116, 2624–2633. https://doi.org/10.1073/pnas.1815014116.

Diniz-Filho, J.A.F., Soares, T.N., Lima, J.S., Dobrovolski, R., Landeiro, V.L., Telles, M.P. de C., Rangel, T.F., Bini, L.M., 2013. Mantel test in population genetics. Gen. Mol. Biol. 36, 475–485. https://doi.org/10.1590/S1415-47572013000400002.

Esquerré, D., Donnellan, S., Brennan, I.G., Lemmon, A.R., Lemmon, E.M., Zaher, H., Grazziotin, F.G., Keogh, J.S., 2020. Phylogenomics, biogeography, and morphometrics reveal rapid phenotypic evolution in pythons after crossing Wallace's Line. Syst. Biol. 1–13 https://doi.org/10.1093/sysbio/syaa024.

Esquerré, D., Keogh, J.S., 2016. Parallel selective pressures drive convergent diversification of phenotypes in pythons and boas. Ecol. Lett. 19, 800–809. https://doi.org/10.1111/ele.12620.

Esquerré, D., Ramírez-Alvarez, D., Pavón-Vázquez, C.J., Troncoso-Palacios, J., Garín, C. F., Keogh, J.S., Leaché, A.D., 2019. Speciation across mountains: Phylogenomics, species delimitation and taxonomy of the *Liolaemus leopardinus* clade (Squamata, Liolaemidae). Mol. Phylogenet. Evol. 139, 106524 https://doi.org/10.1016/j.ympev.2019.106524.

Esquerré, D., Sherratt, E., Keogh, J.S., 2017. Evolution of extreme ontogenetic allometric diversity and heterochrony in pythons, a clade of giant and dwarf snakes. Evolution 71, 2829–2844. https://doi.org/10.1111/evo.13382.

Fišer, C., Robinson, C.T., Malard, F., 2018. Cryptic species as a window into the paradigm shift of the species concept. Mol. Ecol. 27, 613–635. https://doi.org/10.1111/mec.14486.

Flouri, T., Jiao, X., Rannala, B., Yang, Z., 2018. Species tree inference with BPP using genomic sequences and the multispecies coalescent. Mol. Biol. Evol. 35, 2585–2593. https://doi.org/10.1093/molbev/msy147.

Frichot, E., Mathieu, F., Trouillon, T., Bouchard, G., François, O., 2014. Fast and efficient estimation of individual ancestry coefficients. Genetics 196, 973–983. https://doi.org/10.1534/genetics.113.160572.

Gavrilets, S., Li, H., Vose, M.D., 2000. Patterns of parapatric speciation. Evolution 54, 1126–1134. https://doi.org/10.1111/j.0014-3820.2000.tb00548.x.

Georges, A., Gruber, B., Pauly, G.B., White, D., Adams, M., Young, M.J., Kilian, A., Zhang, X., Shaffer, H.B., Unmack, P.J., 2018. Genomewide SNP markers breathe new life into phylogeography and species delimitation for the problematic short-necked turtles (Chelidae: *Emydura*) of eastern Australia. Mol. Ecol. 27, 5195–5213. https://doi.org/10.1111/mec.14925.

Greer, A.E., 1997. The biology and evolution of Australian snakes. Surrey Beatty & Sons Pty Limited, Chipping Norton, Australia.
Gruber, B., Unmack, P.J., Berry, O.F., Georges, A., 2018. dartr: An R package to facilitate analysis of SNP data generated from reduced representation genome sequencing. Mol. Ecol. Res. 18, 691–699. https://doi.org/10.1111/1755-0998.12745.
Harvey, M.G., Smith, B.T., Glenn, T.C., Faircloth, B.C., Brumfield, R.T., 2016. Sequence capture versus restriction site associated DNA sequencing for shallow systematics. Syst. Biol. 65, 910–924. https://doi.org/10.1093/sysbio/syw036.
Hillis, D.M., 2019. Species delimitation in herpetology. J. Herpetol. 53, 3–11. https://doi.org/10.1670/18-123.
Hoang, D.T., Chernomor, O., Haeseler, von A., Minh, B.Q., Vinh, L.S., 2018. UFBoot2: Improving the ultrafast bootstrap approximation. Mol. Biol. Evol. 35, 518–522. https://doi.org/10.1093/molbev/msx281.
Isaac, N., Mallet, J., Mace, G.M., 2004. Taxonomic inflation: its influence on macroecology and conservation. Trends Ecol. Evol. 19, 464–469. https://doi.org/10.1016/j.tree.2004.06.004.
Jackson, N.D., Carstens, B.C., Morales, A.E., O'Meara, B.C., 2017. Species delimitation with gene flow. Syst. Biol. 66, 799–812. https://doi.org/10.1093/sysbio/syw117.
Kalyaanamoorthy, S., Minh, B.Q., Wong, T.K.F., Haeseler, von A., Jermiin, L.S., 2017. ModelFinder: fast model selection for accurate phylogenetic estimates. Nat. Methods 14, 587–589. https://doi.org/10.1038/nmeth.4285.
Katoh, K., Standley, D.M., 2013. MAFFT multiple sequence alignment software version 7: Improvements in performance and usability. Mol. Biol. Evol. 30, 772–780. https://doi.org/10.1093/molbev/mst010.
Kilian, A., Wenzl, P., Huttner, E., Carling, J., Xia, L., Blois, H., Caig, V., Heller-Uszynska, K., Jaccoud, D., Hopper, C., Aschenbrenner-Kilian, M., Evers, M., Peng, K., Cayla, C., Hok, P., Uszynski, G., 2012. Diversity arrays technology: a generic genome profiling technology on open platforms, in: data production and analysis in population genomics, Methods in Molecular Biology™. Humana Press, Totowa, NJ, Totowa, NJ,, pp. 67–89. https://doi.org/10.1007/978-1-61779-870-2_5.
Klingenberg, C.P., 2016. Size, shape, and form: concepts of allometry in geometric morphometrics. Dev. Genes Evol. 226, 1–25. https://doi.org/10.1007/s00427-016-0539-2.
Kluge, A., 1993. *Aspidites* and the phylogeny of pythonine snakes. Rec. Aust. Mus. 19, 1–77.
Kvist, S., 2013. Barcoding in the dark?: A critical view of the sufficiency of zoological DNA barcoding databases and a plea for broader integration of taxonomic knowledge. Mol. Phylogenet. Evol. 69, 39–45. https://doi.org/10.1016/j.ympev.2013.05.012.
Leaché, A.D., Oaks, J.R., 2017. The utility of single nucleotide polymorphism (SNP) data in phylogenetics. Annu. Rev. Ecol. Evol. Syst. 48, 69–84. https://doi.org/10.1146/annurev.
Leaché, A.D., Zhu, T., Rannala, B., Yang, Z., 2018. The spectre of too many species. Syst. Biol. 25, 1979–2014. https://doi.org/10.1093/sysbio/syy051.
Lê, S., Josse, J., Husson, F., 2008. FactoMineR: An R Package for Multivariate Analysis. J. Stat. Software 25, 1–18. https://doi.org/10.18637/jss.v025.i01.
Macqueen, P., Seddon, J.M., Austin, J.J., Hamilton, S., Goldizen, A.W., 2010. Phylogenetics of the pademelons (Macropodidae: *Thylogale*) and historical biogeography of the Australo-Papuan region. Mol. Phylogenet. Evol. 57, 1134–1148. https://doi.org/10.1016/j.ympev.2010.08.010.
Mahony, M., Moses, B., Mahony, S.V., Lemckert, F.L., Donnellan, S., 2020. A new species of frog in the *Litoria ewingii* species group (Anura: Pelodryadidae) from south-eastern Australia. Zootaxa 4858, 201–230. https://doi.org/10.11646/zootaxa.4858.2.3.
Mallet, J., 2008. Hybridization, ecological races and the nature of species: empirical evidence for the ease of speciation. Phil. Trans. Roy. Soc. B: Biol. Sci. 363, 2971–2986. https://doi.org/10.1098/rstb.2008.0081.
McKay, B.D., Mays Jr., H.L., Yao, C.-T., Wan, D., Higuchi, H., Nishiumi, I., 2014. Incorporating color into integrative taxonomy: analysis of the varied tit (*Sittiparus varius*) complex in East Asia. Syst. Biol. 63, 505–517. https://doi.org/10.1093/sysbio/syu016.
Miller, S.A., Dykes, D.D., Polesky, H.F., 1988. A simple salting out procedure for extracting DNA from human nucleated cells. Nucleic Acids Res. 16, 1215.
Minh, B.Q., Hahn, M., Lanfear, R., 2018. New methods to calculate concordance factors for phylogenomic datasets. bioRxiv 1–7. doi:10.1101/487801.
Moritz, C., Cicero, C., 2004. DNA barcoding: promise and pitfalls. PLoS Biol. 2, e354.
Moritz, C., Ens, E.J., Potter, S., Catullo, R.A., 2013. The Australian monsoonal tropics: An opportunity to protect unique biodiversity and secure benefits for Aboriginal communities. Pac. Conserv. Biol. 19, 343–355. https://doi.org/10.1071/pc130343.
Mulcahy, D.G., 2008. Phylogeography and species boundaries of the western North American Nightsnake (*Hypsiglena torquata*): Revisiting the subspecies concept. Mol. Phylogenet. Evol. 46, 1095–1115. https://doi.org/10.1016/j.ympev.2007.12.012.
Murphy, J.C., Henderson, R.W., 1997. Tales of giant snakes. Krieger Publishing Company, Malabar, FL, USA.
Natusch, D.J.D., Esquerré, D., Lyons, J.A., Hamidy, A., Lemmon, A.R., Lemmon, E.M., Riyanto, A., Keogh, J.S., Donnellan, S., 2020. Species delimitation and systematics of the green pythons (*Morelia viridis* complex) of Melanesia and Australia. Mol. Phylogenet. Evol. 142, 106640 https://doi.org/10.1016/j.ympev.2019.106640.
Natusch, D.J.D., Lyons, J.A., 2011. The harvest of *Antaresia maculosa* (Pythonidae) from West Papua, Indonesia. Herpetol. Rev. 42, 509–511.
Nguyen, L.-T., Schmidt, H.A., Haeseler, von A., Minh, B.Q., 2015. IQ-TREE: A fast and effective stochastic algorithm for estimating maximum-likelihood phylogenies. Mol. Biol. Evol. 32, 268–274. https://doi.org/10.1093/molbev/msu300.
O'Shea, M., Sprackland, R.G., Bigilale, I.H., 2004. First record for the genus *Antaresia* (Squamata: Pythonidae) from Papua New Guinea. Herpetol. Rev. 35, 225–227.
Oliver, P.M., Prasetya, A.M., Tedeschi, L.G., Fenker, J., Ellis, R.J., Doughty, P., Moritz, C., 2020. Crypsis and convergence: integrative taxonomic revision of the *Gehyra australis* group (Squamata: Gekkonidae) from northern Australia. PeerJ 8, e7971. https://doi.org/10.7717/peerj.7971.
Orr, H.A., Orr, L.H., 1996. Waiting for speciation: the effect of population subdivision on the time of speciation. Evolution 50, 1742–1749. https://doi.org/10.1111/j.1558-5646.1996.tb03561.x.
Padial, J.M., Miralles, A., la Riva, De I., Vences, M., 2010. The integrative future of taxonomy. Front. Zool. 7, 1–14. https://doi.org/10.1186/1742-9994-7-16.
Papakostas, S., Michaloudi, E., Proios, K., Brehm, M., Verhage, L., Rota, J., Peña, C., Stamou, G., Pritchard, V.L., Fontaneto, D., Declerck, S.A.J., 2016. Integrative taxonomy recognizes evolutionary units despite widespread mitonuclear discordance: evidence from a rotifer cryptic species complex. Syst. Biol. 65, 508–524. https://doi.org/10.1093/sysbio/syw016.
Peter, B.M., 2017. rangexpansion. Available at https://github.com/BenjaminPeter/rangeexpansion.
Peter, B.M., Slatkin, M., 2015. The effective founder effect in a spatially expanding population. Evolution 69, 721–734. https://doi.org/10.1111/evo.12609.
Peter, B.M., Slatkin, M., 2013. Deetecting range expansions from genetic data. Evolution 67, 3274–3289. https://doi.org/10.1111/evo.12202.
Potter, S., Bragg, J.G., Peter, B.M., Bi, K., Moritz, C., 2016. Phylogenomics at the tips: inferring lineages and their demographic history in a tropical lizard, *Carlia amax*. Mol. Ecol. 25, 1367–1380. https://doi.org/10.1111/mec.13546.
Pyron, R.A., Burbrink, F.T., Wiens, J.J., 2013. A phylogeny and revised classification of Squamata, including 4161 species of lizards and snakes. BMC Evol. Biol. 13, 1–53.
Pyron, R.A., Hsieh, F.W., Lemmon, A.R., Lemmon, E.M., Hendry, C.R., 2016. Integrating phylogenomic and morphological data to assess candidate species-delimitation models in brown and red-bellied snakes (*Storeria*). Zool. J. Linnean Soc. 177, 937–949. https://doi.org/10.1111/zoj.12392.
Rannala, B., Yang, Z., 2003. Bayes estimation of species divergence times and ancestral population sizes using DNA sequences from multiple loci. Genetics 164, 1645–1656. https://doi.org/10.1006/tpbi.1999.1447.
Rawlings, L.H., Donnellan, S.C., 2003. Phylogeographic analysis of the green python, *Morelia viridis*, reveals cryptic diversity. Mol. Phylogenet. Evol. 27, 36–44. https://doi.org/10.1016/S1055-7903(02)00396-2.
Rawlings, L.H., Rabosky, D.L., Donnellan, S.C., Hutchinson, M.N., 2008. Python phylogenetics: inference from morphology and mitochondrial DNA. Biol. J. Linnean Soc. 93, 603–619.
Reynolds, G.R., Niemiller, M.L., Revell, L.J., 2014. Toward a tree-of-life for the boas and pythons: Multilocus species-level phylogeny with unprecedented taxon sampling. Mol. Phylogenet. Evol. 71, 201–213. https://doi.org/10.1016/j.ympev.2013.11.011.
Rousset, F., 2000. Genetic differentiation between individuals. J. Evol. Biol. 13, 58–62.
Sexton, J.P., Hangartner, S.B., Hoffmann, A.A., 2013. Genetic isolation by environment or distance: which pattern of gene flow is most common? Evolution 68, 1–15. https://doi.org/10.1111/evo.12258.
Shine, R., Slip, D.J., 1990. Biological aspects of the adaptive radiation of Australasian pythons (Serpentes: Boidae). Herpetologica 46, 283–290.
Shirley, M.H., Vliet, K.A., Carr, A.N., Austin, J.D., 2014. Rigorous approaches to species delimitation have significant implications for African crocodilian systematics and conservation. Proc. R. Soc. B. 281, 20132483. https://doi.org/10.1098/rspb.2013.2483.
Singhal, S., Hoskin, C.J., Couper, P., Potter, S., Moritz, C., 2018. A framework for resolving cryptic species: a case study from the lizards of the Australian Wet Tropics. Syst. Biol. 67, 1061–1075. https://doi.org/10.1093/sysbio/syy026.
Sites, J.W., Marshall, J.C., 2004. Operational criteria for delimiting species. Annu. Rev. Ecol. Evol. Syst. 35, 199–227. https://doi.org/10.1146/annurev.ecolsys.35.112202.130128.
Smith, L.A., 1985. A revision of the *Liasis childreni* species group (Serpentes: Boidae). Rec. West. Aust. Mus. 12, 257–276.
Solís-Lemus, C., Knowles, L.L., Ané, C., 2015. Bayesian species delimitation combining multiple genes and traits in a unified framework. Evolution 69, 492–507. https://doi.org/10.1111/evo.12582.
Soubrier, J., Steel, M., Lee, M.S.Y., Sarkissan, C.D., Guindon, S., Ho, S.Y.W., Cooper, A., 2012. Influence of rate heterogeneity among sites on the time dependence of molecular rates. Mol. Biol. Evol. 29, 3345–3358. https://doi.org/10.1093/molbev/mss140.
Spinks, P.Q., Thomson, R.C., Shaffer, H.B., 2014. The advantages of going large: genome-wide SNPs clarify the complex population history and systematics of the threatened western pond turtle. Mol. Ecol. 23, 2228–2241. https://doi.org/10.1111/mec.12736.
Stekhoven, D.J., Bühlmann, P., 2012. MissForest–non-parametric missing value imputation for mixed-type data. Bioinformatics 28, 112–118. https://doi.org/10.1093/bioinformatics/btr597.
Sukumaran, J., Knowles, L.L., 2017. Multispecies coalescent delimits structure, not species. Proc Natl Acad Sci U S A 114, 1607–1612. https://doi.org/10.1073/pnas.1607921114.
Swofford, D.L., 2003. PAUP*. Phylogenetic analysis using parsimony (* and other methods). Version 4.
Tajima, F., 1989. Statistical method for testing the neutral mutation hypothesis by DNA polymorphism. Genetics 123, 585–595.
Torr, G., 2000. Pythons of Australia: a natural history. Krieger Publishing co., Malabar, FL, USA.
Underwood, G., Stimson, A.F., 1990. A classification of the pythons (Serpentes, Pythonidae). J. Zool. 221, 565–603.
Voris, H.K., 2000. Maps of Pleistocene sea levels in Southeast Asia: shorelines, river systems and time durations. J. Biogeogr. 27, 1153–1167. https://doi.org/10.1046/j.1365-2699.2000.00489.x.

Williams, D., 1992. "Natural" incubation by a Children's python, *Liasis maculosus* (Peters, 1873) (Serpentes: Boidae), under public display conditions. Sydney Basin Naturalist 1, 97–99.

Yoder, A.D., Campbell, C.R., Blanco, M.B., Reis, dos M., Ganzhorn, J.U., Goodman, S.M., Hunnicutt, K.E., Larsen, P.A., Kappeler, P.M., Rasoloarison, R.M., Ralison, J.M., Swofford, D.L., Weisrock, D.W., 2016. Geogenetic patterns in mouse lemurs (genus Microcebus) reveal the ghosts of Madagascar's forests past. Proc. Natl. Acad. Sci. U. S.A. 113, 8049–8056. https://doi.org/10.1073/pnas.1601081113.

Yokoyama, Y., Purcell, A., Lambeck, K., Johnston, P., 2001. Shore-line reconstruction around Australia during the Last Glacial Maximum and Late Glacial Stage. Quat. Int. 83–85, 9–18. https://doi.org/10.1016/S1040-6182(01)00028-3.

Zozaya, S.M., Macdonald, S.L., 2013. Snakes of Australia (1.0.4) [Mobile application software]. Retrieved from http://www.ugmedia.com.au.